Electrical Power

10

Mukund R. Patel

10.1 Power System Basics

The electrical power system (EPS) generates, stores, conditions, controls, and distributes power within the specified voltage band to all bus and payload equipment. The protection of the power system components in case of all credible faults is also included. The basic components of the most widely used power system are (1) solar array, (2) solar array drive, (3) battery, (4) battery charge and discharge regulators, (5) bus voltage regulator, and (6) switches, fuses, and distribution harness.

Power requirements in very early satellites were several watts. In today's communication satellites, it can be 20 kW or higher. Some strategic defense spacecraft power requirement may be in hundreds of kilowatts and some defense concepts require hundreds of megawatts of burst power. Solar radiation is the only external source of primary energy available in space with reasonable flight heritage, although other concepts such as conductive wires have been considered. Any spacecraft not using solar energy must carry on-board its own source of energy, such as the primary battery, radioisotope, nuclear reactor, or chemical fuel. The conversion of the primary energy into electrical energy may be photovoltaic (PV), thermoelectric (TE), dynamic alternator, or thermionic. Some energy storage may also be required in many spacecraft to meet the load power requirement during eclipse or during any peak demand period. Energy storage has been primarily by electrochemical battery, although regenerative fuel cell and flywheel technologies are under development.

From available options that are compatible with a given mission and its environment, the satellite-level optimization study determines the best combination of primary energy source, energy conversion, and energy storage technologies. Final selection must meet multiple criteria, but the primary criteria are always low mass and low life cycle cost. Such selection is largely influenced by the power level × mission duration product as shown in Fig. 10.1, where the dividing lines among various options have large overlaps. Although the PV-battery power system is the most common for Earth-orbiting satellites, a variety of alternative power system technologies have been developed and flown for various space missions [1]. The practical limit and performance characteristics of major power system options are summarized in Table 10.1.

The U.S. Department of Defense and NASA have also funded the development and testing of proto-flight solar array designs that could yield a specific power of over 100 W/kg, a factor of 3 greater than the state of the art and a factor of 5 greater than the state of the practice. The advanced designs under consideration integrate three promising technologies [2]: (1) flexible copper indium diselenide thin-film PV cells, (2) smart mechanisms using shape memory metal, and (3) multi-functional lightweight structures. An important criterion in application of a new technology is the flight qualification status. Any new component is subject to time-consuming and expensive testing to prove its ability to withstand launch and space environments.

10.2 Photovoltaic-Battery System

The solar energy and PV-battery power system is widely used in Earth orbiting satellites. The solar flux received from the Sun varies with the distance squared. Earth's orbit around the Sun is approximately circular with a slight eccentricity of 0.01672. The distance, therefore, varies within ±0.01672 times the average distance between the Sun and the Earth, which is 149.6 million km, defined as one astronomical unit (au) of distance. Thus, the solar flux varies

M. R. Patel (✉)
U.S. Merchant Marine Academy, Kings Point, NY, USA

M. Macdonald and V. Badescu (eds.), *The International Handbook of Space Technology*, Springer Praxis Books, DOI: 10.1007/978-3-642-41101-4_10,

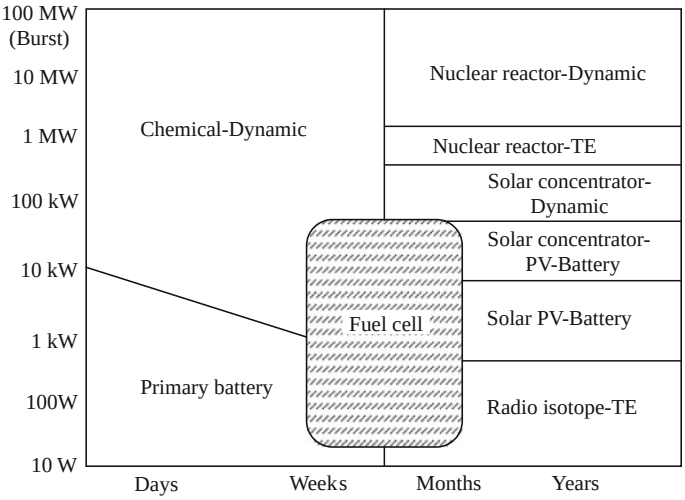

Fig. 10.1 Optimum primary energy sources for various power levels and mission durations

Table 10.1 Practical limit and performance of various power system options

Power system option	Practical power limit (kW)	Net system efficiency (%)	Specific power
Solar-PV	20–30	15–30	5–10 W/kg
Isotope-TE	1	7–15	5–10 W/kg
Nuclear-TE	100–300	7–15	–

over $(1 \pm 0.01672)^2$ or 1 ± 0.034 of the yearly average. For many years, the average solar radiation in Earth orbit was taken as $1{,}358 \pm 5$ W/m^2 on a surface normal to the Sun. Measurements reported by Frohlich [3] showed a higher average value of $1{,}377 \pm 5$ W/m^2, however the conservative number of $(1{,}358 - 5) = 1{,}353$ W/m^2 continues in wide use, particularly for power system sizing. Recall from Sect. 3.2.3 that the ASTM E490 Standard Solar Constant and Zero Air Mass (AM0) Solar Spectral Irradiance has an integrated power of 1,366.1 W/m^2; an ISO standard is also available, see ISO-21348. Since the ecliptic and equatorial planes are inclined to each other by 23.45°, the angle of incidence of the sunlight on an uncontrolled geostationary satellite's solar arrays varies from 66.55° to 90°. The corresponding incident solar flux varies from 91.75 % on a solstice day to 100 % on an equinox day. However, the satellite on equinox days encounters the longest eclipse once per day when the Earth blocks the sunlight from illuminating the satellite.

Alternative PV-battery architectures are depicted in Fig. 10.2. The direct energy transfer (DET) from the solar array to the load is best for the overall system efficiency. In the DET category are (1) a sunlight regulated bus in which the excess solar array current (if any during sunlight) is shunted to the ground in order to maintain the bus voltage in a narrowband and the bus voltage during eclipse is the battery voltage. And, (2) a fully regulated bus in which the bus voltage is regulated within a narrowband during the entire orbit. The other option is (3) a peak power tracking (PPT) architecture in which a series regulator matches the load and the source characteristics to extract the maximum power from the solar array. Power loss of several percent in the PPT regulator sometimes nullifies the gain in power from solar array. The PPT architecture may be suitable for a mission operating over wide orbit parameters. However, the sunlight or fully regulated bus generally leads to the optimized design for large high-power satellites.

10.2.1 Solar Array

The solar array is made of numerous PV cells mounted on a base substrate and connected in a series–parallel combination to obtain the desired voltage and current. Each cell can be of any of the following types: (1) single crystal silicon, (2) gallium arsenide, (3) semi-crystalline or polycrystalline, (4) thin film, (5) amorphous, or (6) multi-junction. As of 2012, a new class of ultra-light, high-efficiency solar cell has been developed by the U.S. Department of Energy. It is the inverted metamorphic multijunction (IMM) with the conversion efficiency of 42.3 ± 2.5 % as measured by the U.S. National Renewable Energy Laboratory. The tests were made on *InGaP/GaAs/InGaAs* three-junction cells with concentration of 406 Suns on Earth (atmospheric mass, AM, 1.5) and cell temperature of 250 °C [4]. These cells consist of multiple thin films in layers that allow the cell to capture more of the solar spectrum and convert it into electrical power. The maximum reported efficiency is slightly better than 41.4 % achieved by the Fraunhofer Institute for Solar Energy Systems.

The IMM cells, primarily developed for terrestrial applications at present, are also developed for the space satellite market by companies like Emcore and Spectrolab. The IMM solar array in space without concentration could

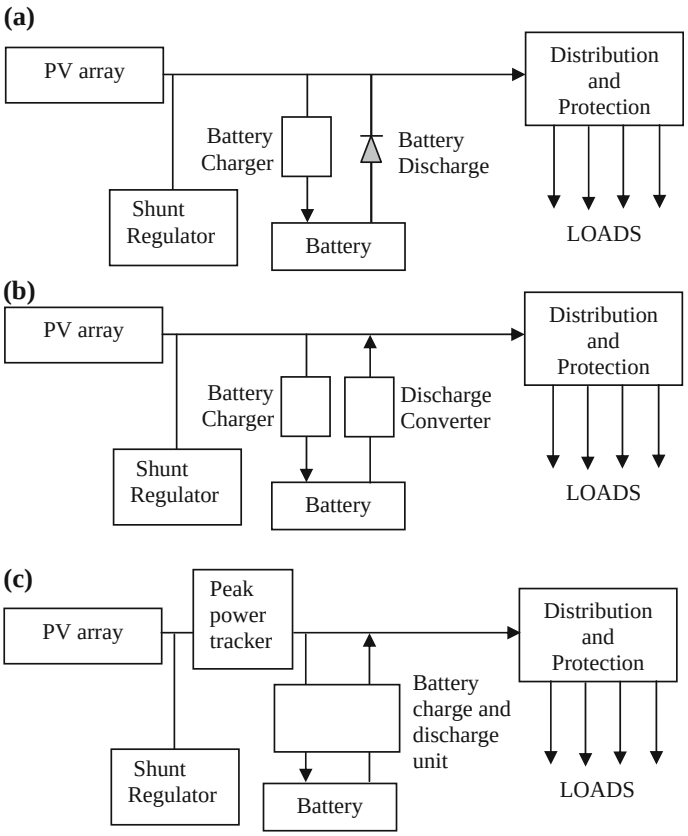

Fig. 10.2 Alternative architectures for spacecraft power. **a** DET-sunlight regulated bus. **b** DET-fully regulated bus. **c** Peak power tracking bus

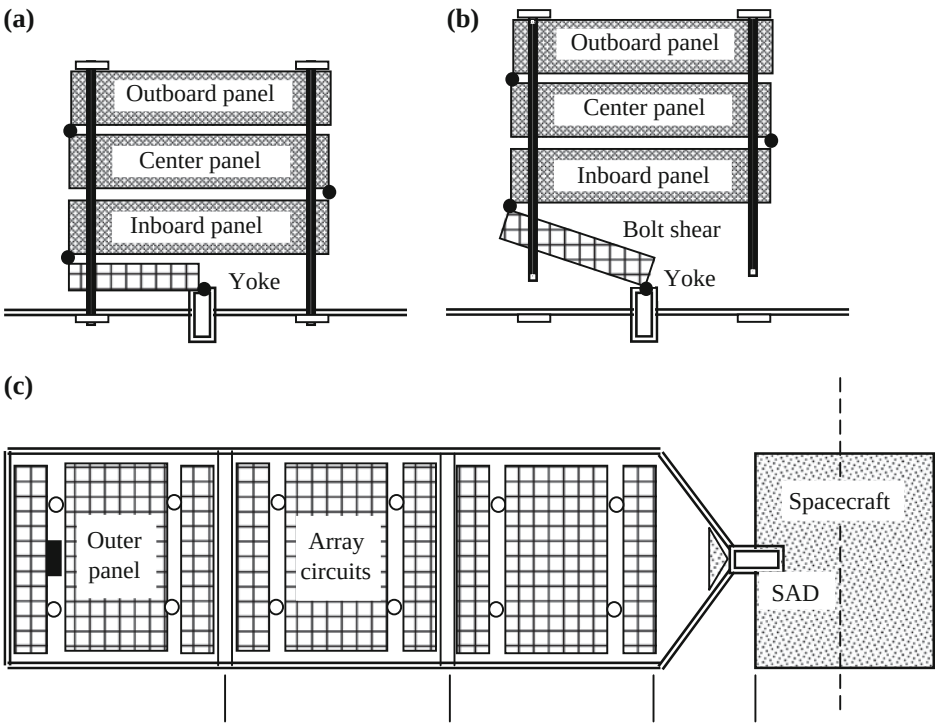

Fig. 10.3 Flat panel soar array wing: **a** stowed (array is held in place by four hold-down release devices during launch and transfer orbit), **b** being deployed (four hold-down release devices are actuated when final orbit is achieved and yoke begins to unfold), and **c** fully deployed (after center panel is fully outfolded and locked, the outboard panel fully unfolds and locks. Hinge position microswitches send the array-deployed signal)

be 33–35 % efficient and be incorporated into a satellite's skin or unfurl like an awning. This would eliminate the need for conventional wing-shaped solar arrays with heavy metal frames and associated mechanisms.

Solar array construction can be (1) rigid flat panels, (2) body mounted panels, (3) flexible blanket type array, (4) inflatable balloon type array, or (5) concentration array. Most arrays are made with crystalline silicon or gallium

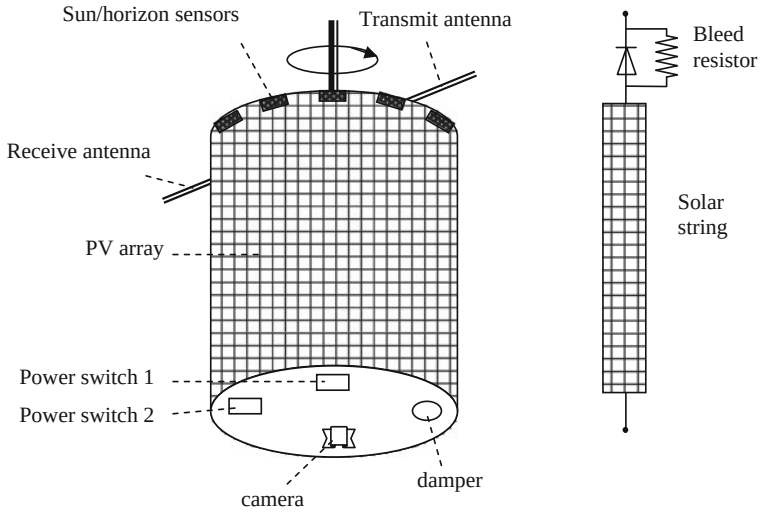

Fig. 10.4 Body mounted solar array with bleed resistor in each solar string

Table 10.2 Key features of 3-axis stabilized and spin-stabilized satellites

3-axis stabilized flat wings	Spin-stabilized round body
Bias or zero momentum maintains the stability	Inherently stiff due to rotational inertia
Complex attitude control	Simple mechanical structure
Full solar array normal to the Sun generates power all the time	Only 1/3rd of the solar array generates power at any time
Can have high power by adding solar panels on wings	Power limited by body size that fits the launch vehicle
Great flexibility in design	Less flexibility in design
Suitable for large satellites	Suitable for small satellites

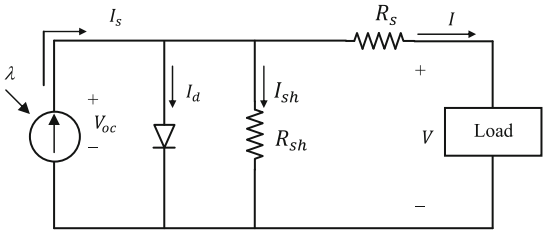

Fig. 10.5 Equivalent electrical circuit of solar cell

arsenide cells on rigid panels, where the solar panels can be flat wings (Fig. 10.3) in 3-axis stabilized spacecraft, or mounted on a round body surface (Fig. 10.4) in spin-stabilized spacecraft. The key features of these two basic types of solar panels are given in Table 10.2.

The steady state equivalent electrical circuit of a PV cell (and also of a PV panel by series–parallel scaling) is shown in Fig. 10.5. The cell acts as a constant current source shunted by a diode. In the circuit parameters, the series resistance R_s represents the internal resistance to the current flow, which is primarily due to the resistivity of the material. The shunt resistance represents the leakage current across the junction. It depends on the p-n junction depth, the impurities, and the contact resistance. The value of R_{sh} is inversely related with the leakage current to ground. In an ideal PV cell, $R_s = 0$ (no series loss), and $R_{sh} = \infty$ (no leakage to ground). In a typical high quality 2.0 × 2.5 cm silicon cell, $R_s = 0.05$–$0.10\ \Omega$ and $R_{sh} = 200$–$300\ \Omega$. The PV conversion efficiency is sensitive to small variations in R_s, but is insensitive to variations in R_{sh}. The value of R_{sh} affects the constant current slope, whereas the value of R_s affects the constant voltage slope. A small increase in R_s can decrease the PV output significantly. Since the magnitudes of the diode current and the resistances R_s and R_{sh} vary with temperature, the cell output and the conversion efficiency decrease with increasing temperature.

10.2.1.1 P–V and I–V Characteristics

The current versus voltage (I–V) characteristic of the PV cell in sunlight is shown in Fig. 10.6a, where two important parameters for characterizing the cell performance are the open circuit voltage V_{oc} and the short circuit current I_{sc}. The short circuit current is measured by shorting the output terminals and measuring the terminal current under full illumination. Ignoring the small diode and ground leakage currents under zero terminal voltage, I_{sc} is the photocurrent

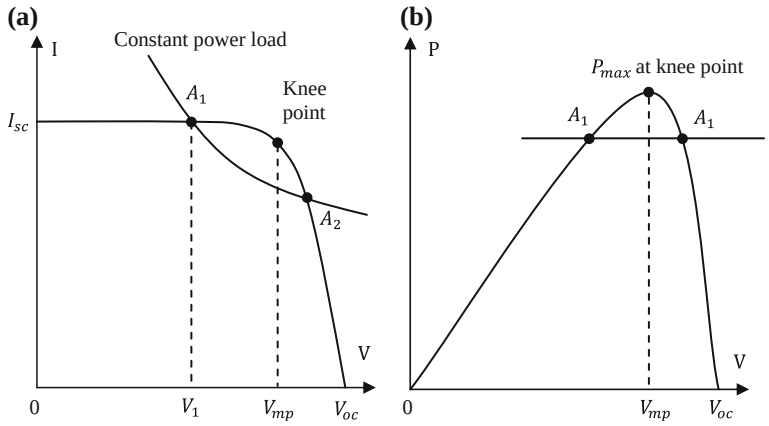

Fig. 10.6 Solar array output characteristics and constant power load curves. **a** I–V characteristic. **b** P–V characteristic

I_s. The current under this condition is the maximum current the cell can deliver. The bottom right of the curve at zero current is the open circuit voltage measured with the output terminals open. The maximum photo voltage is produced under the open circuit voltage. The I–V curves over a full range are developed from the test data at various illuminations, temperatures, and ionized radiation doses.

The product of voltage and current outputs is the output power, which is plotted in Fig. 10.6b. The cell produces no power at zero voltage or zero current, and produces the maximum power at a voltage corresponding to the knee point of the I–V curve. This is why the PV power circuits are designed such that the panel operates closed to the knee-point, slightly on the left-hand side, where the cell operates approximately as a constant current source.

The basic requirements of solar cells for space applications are generally described in MIL-STD-83576 by the U.S. Air Force. The cell specifications for general use in space are defined by AIAA Standards-115 and -116. The ISO Technical Committee C20 has issued ISO-15387 for the aircraft and space vehicles and this is endorsed by American National Standard Institute. NASA's Jet Propulsion laboratory (JPL) often performs such tests in aircraft and balloons at 35 km height. Comparing such tests conducted by one organization with another is difficult. For example, in a round-robin test by six organizations to ISO-15387, including tests conducted at JPL and in the PV engineering test bed at NASA's Glenn Research Center, the results showed up to 3 % deviations on the same cell. The cell temperature coefficient is extremely sensitive to solar spectrum, and can vary several fold, making the spectrum duplication in tests extremely important. For this reason, power engineers allow 3 % margin for standard cells, and perhaps more for multi-junction cells, as the possible error in power generation estimates using the test results.

10.2.1.2 Array Performance

Major factors influencing the electrical performance of the solar array are solar intensity, Sun angle, and the operating temperature. The I–V characteristic of a PV array reduces in

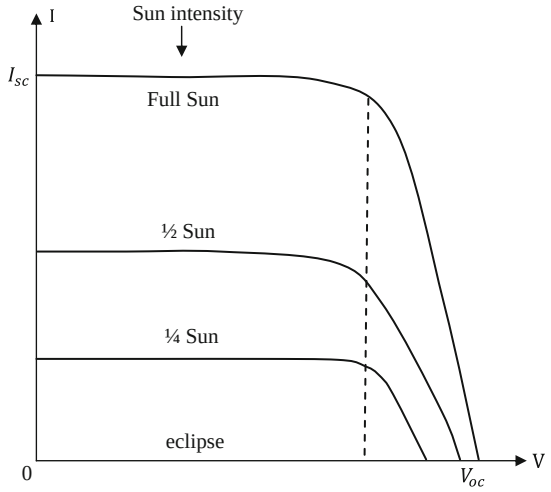

Fig. 10.7 Solar array current versus voltage at various illumination levels

magnitude at lower Sun intensity with a small reduction in voltage a shown in Fig. 10.7. However, the photo conversion efficiency of the cell is insensitive to solar illumination in the practical working range. Figure 10.8 shows that the efficiency is practically the same at full Sun (1,353 W/m^2) and 1/2 Sun, and starts to fall off rapidly only below 1/4 Sun (340 W/m^2).

The cell output current is given by $I_s = I_0 \cos\theta$, where I_0 is the photocurrent with normal Sun ($\theta = 0$). The cosine law holds well for Sun angles ranging from 0 to about 50°, beyond which the electrical output deviates significantly from the cosine value. The cell generates no power beyond 85°, although the mathematical prediction would give 7.5 % power generation. The actual power versus angle curve is called the Kelly cosine, which is useful to assess accurately the power available from the Sun at low angles during transfer orbit.

With increasing temperature, the short circuit current of the cell increases, whereas the open circuit voltage decreases as shown in Fig. 10.9; as the increase in current is much less than the decrease in voltage, the net effect is the decrease in

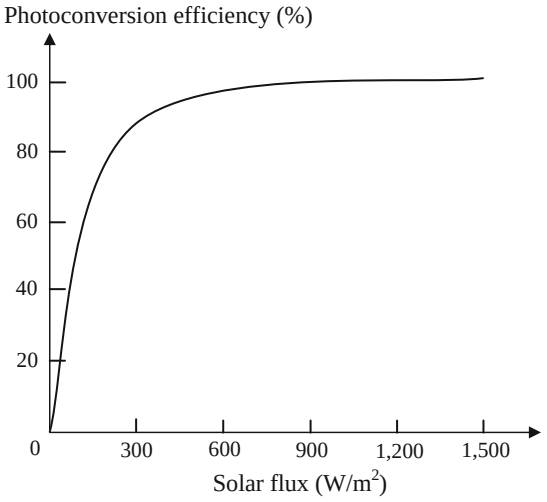

Fig. 10.8 Photoconversion efficiency remains constant over wide range of solar flux up to 1/4 Sun

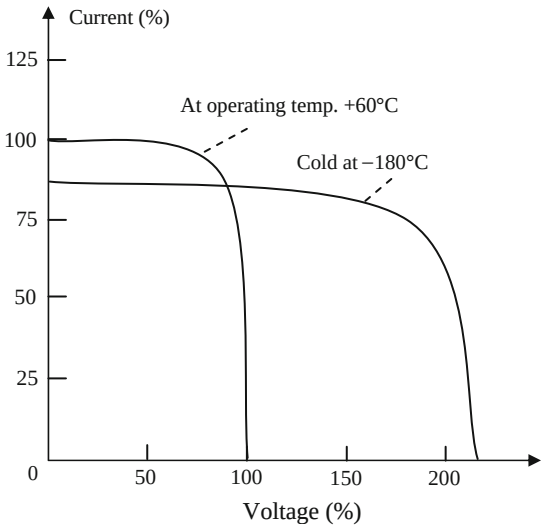

Fig. 10.9 Temperature effect on I–V curve of solar array

power, which is quantitatively evaluated by examining the effects on current and voltage separately. Say that I_0 and V_0 are the short circuit current and the open circuit voltage at reference temperature T, and α and β are their temperature coefficients in units of A/°C and V/°C, respectively. If the operating temperature is increased by ΔT, then the new current and voltage are given by $I_{sc} = (I_0 + \alpha\Delta T)$ and $V_{oc} = (V_0 + \beta\Delta T)$. Since the operating current and voltage change approximately in the same proportion as the short circuit current and open circuit voltage, respectively, the new power $P = V\,I = (I_0 + \alpha\,\Delta T) \cdot (V_0 + \beta\Delta T)$. Ignoring the small term containing the product of α and β, $P = V_0 I_0 + \alpha\Delta T\mathrm{V}_0 - \beta\Delta T I_0$, which reduces to a simple form

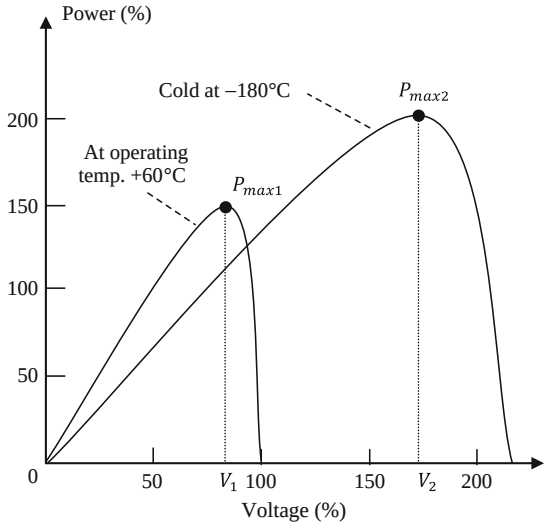

Fig. 10.10 Temperature effects on P–V curve of solar array

$$P = P_0 - [(\alpha \mathrm{V}_0 - \beta I_0)\Delta T]r^n = 0.4 + 0.3(2^n). \quad (10.1)$$

For a typical 2 × 4 cm single-crystal silicon cell, α is 250 μA/°C and β is 2.25 mV/°C. Therefore, the power varies approximately as $P = P_0(1 - 0.005\Delta T)$, which indicates that for every 1 °C rise in the operating temperature, the silicon cell power output decreases by about 0.50 %.

Figure 10.10 depicts the power output versus voltage characteristic at two operating temperatures. It shows that the maximum power generated at the lower temperature is higher. Thus, cold temperatures are better for the PV cell for power generation. However, the two P_{max} points are not at the same voltage. In order to extract maximum power at all temperatures, the PV system must be designed such that the array output voltage can increase to V_2 for capturing P_{max2} at lower temperature, and can decrease to V_1 for capturing P_{max1} at higher temperatures. If the array is operating at a fixed regulated voltage, the higher power generation capability at cold temperatures cannot be utilized by the loads, and the excess power from the cell must be wasted in shunt circuits. The peak power all the time, regardless of the temperature, can be captured and utilized only by using the PPT architecture.

The array undergoes a wide temperature cycle in each orbit. During sunlight, the front face rises to 50–60 °C and the back face to 40–50 °C. The solar array temperature is determined by the thermal equation: (Solar flux + Earth's albedo + Earth's thermal radiation + Heat coming from adjacent components of the spacecraft) = (Electrical power output + Heat radiated back into space). During eclipse in GEO, the temperature drops exponentially to as low as − 175 °C. The time constant depends on the mass composition of the array components, and is typically 30–60 min. The front to back face temperature gradient for a rigid array with face sheets made of either aluminum (obsolete) or

Table 10.3 Degradation factors for 900 W satellite with a 15 year operational life in medium Earth orbit; 10,900 nm, 69° inclination; GPS II F orbit

I_{sc} factors	
Natural radiation[a]	
Assembly mismatch loss[b]	0.98
Cover glass charge particles	0.99
Cover glass coating (ITO)[b]	0.98
Ultraviolet rays	0.97
Propellant contamination	0.98
Micrometeoroid damage	0.98
V_{oc} factors	
Natural radiation[a]	
Cover glass charge particles	0.99
P_{max} factors	
Natural radiation[c]	
Wiring loss (cell-to-cell)[b]	0.98

[a] Determined from the radiation fluence over the mission life
[b] Beginning of life
[c] Approximate value equal to the product of the I_{sc} and V_{oc} degradation factors can be used in top-level calculations only. In detailed calculations, it is accounted through the I_{sc} and V_{oc} factors

graphite epoxy (new designs) can be 5–10 °C under steady Sun and up to 20 °C on sunlight snap after eclipse. Various techniques are used to control the temperature of spacecraft parts over a full orbit. Figure 10.9 indicates that a typical cold array facing the Sun immediately after coming out of a long eclipse in GEO develops about twice its normal operating voltage in steady sunlight.

Solar array performance degrades due to two distinct groups of factors. In the first group are the initial degradations at beginning-of-life (BOL) due to (1) cell mismatch in the assembly, (2) cell-to-cell wiring loss, (3) power loss in array and boom wires, and (4) plasma effects that cause leakage current from the array to space. In the second group are the accumulated degradations up to the end-of-life (EOL) due to various environmental effects, such as (1) cumulative radiation dose of the ionized particles, (2) effect of ultraviolet rays on the optical properties of cover glass, (3) mechanical stress cycles causing soldered joints to crack over time, (4) impacts of micrometeoroids and debris damaging solder joints and reducing power generating area of the cells, (5) flue gases changing the optical properties of cover glass, (6) bypass diode failure causing loss in the string current. Table 10.3 gives representative values of major degradation factors for a typical medium Earth orbit, from which the total degradation can be obtained as

$$\text{Total degradation} = \text{BOL degradation} + \text{In-service degradation to EOL}. \tag{10.2}$$

10.2.1.3 Peak Power Tracking

Sun tracking is required in order for the solar array to face the Sun continuously as the spacecraft orbits the Earth. This is done by an actuator that follows the Sun like a sunflower. There are two types of Sun trackers: (1) single-axis gimbals, which follow the Sun from east to west during the day, and (2) dual-axis gimbals that track the Sun from east to west during the day and from north to south during the seasons of the year. The dual axis tracking is done by two linear actuator motors, which aim at the Sun within 1° of accuracy. The EPS provides a means of independently orienting and rotating the deployed north and south solar wings about the pitch axis of the spacecraft. After the deployment, ground control is involved in aligning the solar array to the Sun. Once aligned, the array rotates by the clock time without ground intervention to maintain the Sun orientation. Some Sun pointing error cannot be avoided even after acquiring the normal Sun by the Sun sensor and then tracking by the solar array drive. The error generally comes from the cell flatness error of about 2° and the gimbal tolerance error of about 3°. The total 5° error must be accounted for in the array design. The cosine of 5° is 0.996, which means a 5° Sun pointing error will reduce the power generation by 0.4 %.

The gimbal's motor drives the array module to face the Sun to collect the maximum solar flux. However, that alone does not guarantee the maximum power output from the module. The module must electrically operate at the voltage that corresponds to the peak power point P_{max} under the given operating conditions. If the array is operating at voltage V and current I on the I–V curve, the power generation is $P = VI$ watts. If the operation moves away from the above point, such that the current is now $(I + \Delta I)$, and the voltage is $(V + \Delta V)$, the new power is $P + \Delta P = (V + \Delta V)(I + \Delta I)$. After ignoring a small term, this equation simplifies to $\Delta P = (\Delta VI + \Delta IV)$. The ΔP should be zero at the peak power point, which necessarily lies on a locally flat neighborhood as shown in Fig. 10.6b. Therefore

$$At\, P_{max}\, point, \frac{dP}{dV} = 0,\ which\, reduces\, to \frac{dV}{dI} = -\frac{V}{I}. \tag{10.3}$$

Note that (dV/dI) is the dynamic impedance and (V/I) is the static impedance of the PV array, and the P_{max} point is at the knee-point shown in Fig. 10.6a.

10.2.2 Battery

Energy storage is required in order to meet the spacecraft load demand during the launch/injection phase, during

eclipses, and when the demand exceeds the power generation at any time. The most widely used energy storage technology is the rechargeable battery that stores energy in electrochemical form. The battery is made of numerous electrochemical cells assembled in series–parallel combination to obtain the required voltage and current. The cell stores energy at a low electrical potential. The cell voltage depends solely on the electrochemistry, and not on the physical size. Commonly used electrochemistries produces 1.5–4.2 V when fully charged. The cell's ampere-hour (Ah) storage capacity, denoted by C, depends on the physical size. It is defined as the Ah charge that the cell can deliver at room temperature until it reaches a cut-off voltage of about two-thirds of the fully charged cell voltage. The battery can deliver C amperes for 1 h or C/n amperes for n hours. The cell capacity measures the Ah output at the terminals, not what is stored between the plates. A 1.5 V cell discharged to 1.0 V delivers practically the full capacity of the cell, and delivers only a few percent more if drained further to 0.1 V.

The battery voltage rating is stated in terms of the average voltage during discharge. A higher-voltage battery requires a greater number of cells in series. The product of voltage and the Ah rating gives the energy rating in watt-hours (Wh) that the battery can deliver to a load from the fully charged state. The battery charge and discharge rates are stated in fractions of the capacity. For example, charging a 100 Ah battery at a 10 A rate is said to be charging at $C/10$ rate. Discharging this battery at $C/2$ rate means drawing 50 A. At this rate, the battery will be fully discharged in 2 h. The battery depth of discharge $DoD = (1 - SoC)$, where

$$SoC = \text{Battery state of charge} = \frac{\text{Ah capacity remaining in the battery}}{\text{Rated Ah capacity}}. \quad (10.4)$$

Major rechargeable batteries used in the spacecraft industry at present are (1) nickel–cadmium (NiCd), (2) nickel-hydrogen (NiH_2), and (3) lithium-ion (Li-ion). New electrochemistries are continuously researched for space applications [5], and for a variety of ground-based applications—consumer electronics, electric vehicles, utility load leveling, and renewable power systems. Lithium-polymer (Li-poly) and nickel-metal-hydride (NiMH) are two such examples in the commercial world.

The following figures of merit are often used in comparing the relative performance of various electrochemistries: (1) specific energy or gravimetric energy density = energy stored per unit mass, Wh/kg, (2) energy density or volumetric energy density = energy stored per unit volume, Wh/L, (3) cycle life = number of charge/discharge cycles the battery can deliver while maintaining the minimum required voltage, and (4) specific power and power density = power the battery can practically deliverer per kilogram of mass and liter of volume, respectively. It is sometimes necessary to think in terms of the power parameters also, since the internal resistances of the battery may limit the rate at which the energy can be discharged within practical design limits.

The NiCd battery has served as the workhorse of the spacecraft industry since the earliest missions, and is still used in some missions. However, since the mid-1980s it has been replaced by NiH_2 in general use due to NiCd's memory effect—loss of capacity after repeated use at low DoD. The NiH_2 provides deeper DoD for comparable cycle life, thus requiring lower Ah capacity, which translates into lighter weight. Today, the industry appears to be moving towards lithium based batteries for potentially 2–5 times the specific energy compared to NiH_2. Lithium-ion has a charge/discharge ratio and a round trip energy efficiency close to unity at low depth of discharge. However, no single electrochemistry can meet the wide range of space mission requirements. All chemistries will perhaps continue in use where they fit the best for a minimum mass and cost design.

10.2.2.1 Battery Performance

The battery works as a voltage source with small internal resistance. Its electrical circuit model has the internal electrochemical voltage E_i with internal resistance R_i in series. The E_i decreases and R_i increases linearly with the Ah discharge. Quantitatively

$$E_i = E_o - K_1 \cdot DoD \quad and \quad R_i = R_o + K_2 \cdot DoD \quad (10.5)$$

where E_0 and R_0 are internal voltage and internal resistance in a fully charged battery with $DoD = 0$, and K_1 and K_2 are electrochemistry constants to be found by curve-fitting the test data. The terminal voltage drops with increasing load current I, such that $V_{Terminal} = E_i - IR_i$, where E_i and R_i are functions of DoD. Thus, the terminal voltage is also a function of DoD as shown in Fig. 10.11 for NiH_2 cell in one full LEO orbit, discharging to various DoD levels during a 36-min eclipse and then fully charging up before the next orbit.

The design and operation of a battery requires certain safety considerations. The most important is not to overcharge the battery. Any overcharge above the trickle charge rate is converted into heat, which can explode the battery if allowed to build up beyond limit. This is particularly critical when the battery is charged directly from a dedicated photovoltaic module without a charge regulator in small science missions with short duration or infrequent eclipses. In such cases, the array rating is kept below the continuous trickle charge current that can be tolerated by the battery.

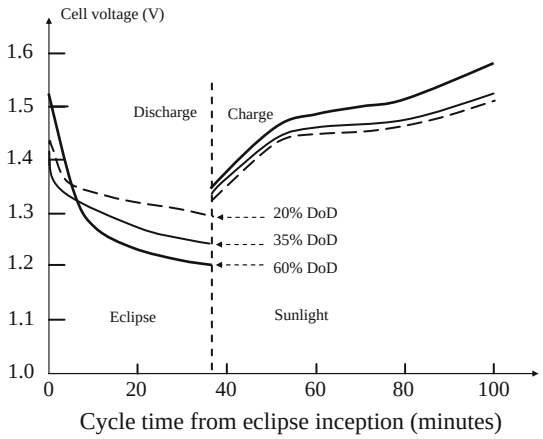

Fig. 10.11 NiH_2 cell voltage during one charge/discharge cycle at various DoD in LEO

10.2.2.2 Battery Life

The battery's primary mode of failure is associated with electrode wear due to repeated charge/discharge cycles. The cycle life depends strongly on the electrochemistry, depth of discharge, and temperature, as depicted in Fig. 10.12 for NiCd and NiH_2 batteries. The battery life also depends to a lesser degree on the electrolyte concentration, electrode porosity, and charge and discharge rates. The electrolyte concentration makes significant difference in the cycle life of NiH_2 cell. The cell with 26 % concentration gives a greater cycle life than one with 31 % concentration.

The number of charge/discharge cycles in a satellite equals the number of eclipses during the mission life. It is at least an order of magnitude greater in LEO than in GEO. Such long cycle life requirement in LEO can be achieved only by limiting the battery design to a low DoD, typically 30 % in LEO as compared to 80 % in GEO. For this reason, a LEO battery is proportionately much larger than a comparable battery in GEO delivering the same Wh energy during each discharge.

It is noteworthy from Fig. 10.12 that the life at given temperature is an inverse function of the depth of discharge. If the life is 100 units at 50 % DoD, then it would be about 200 units at 25 % DoD. The $cycle\ life \times DoD$ product is roughly constant in the first approximation, although it decreases with increasing temperature. Such is true for most electrochemistries. This means that the battery at a given temperature can deliver the same number of equivalent full charges regardless of the depth of discharge. Phrased differently, the total Wh energy that the battery can deliver over its life is roughly constant. The battery lasts proportionately longer if less energy is used per cycle. This observation is useful in comparing the mass and cost of various battery options for a given application at the conceptual design stage.

Once the electrochemistry and the number of parallel batteries are settled, the battery design depends on system parameters such as (1) bus voltage and load current, (2) charge and discharge rates and duration, (3) operating temperature during charge and discharge, and (4) life in terms of number of charge and discharge cycles. The life consideration is the dominant design driver in setting the Ah ratings. Even when the load may be met with a smaller capacity, the battery is oversized to meet the cycle life requirement. For example, with the same Wh load, the battery that must deliver twice as many cycles approximately double the capacity.

The issue of in-orbit battery reconditioning is considered in Chap. 20.

10.2.3 Power Electronics

Major power electronic components used in the spacecraft are (1) shunt regulator for bus voltage control during sunlight, (2) battery charge converter (buck converter), and (3) battery discharge converter (boost converter). They control the bus voltage and convert the voltage to match the operating voltages of various components. The voltage conversion is performed by solid-state semiconductor devices used as controlled switches which are turned on and off at high frequency. Capacitors and inductors are used to store energy when the switch is connected to the power source. The stored energy is then discharged to continue powering the load when the switch is off. Transformers are used where needed.

10.2.3.1 Switching Devices

A variety of solid-state devices are used as controlled switches. However, the devices commonly used in space are (1) metal-oxide semiconducting field effect transistor (MOSFET), (2) bipolar junction transistor (BJT), and (3) insulated gate bipolar transistor (IGBT). The device selection depends on the required voltage, current, and switching frequency. A common feature among these devices is that all are three-terminal devices. Their generally used circuit symbols are shown in Fig. 10.13. The two power terminals 1 and 0 are connected in the main power circuit. The control gate terminal G is connected to the auxiliary control circuit. In normal conducting operation, terminal 1 is generally at higher voltage than terminal 0. Since the device is primarily used for switching power on and off as required, it is functionally represented by a gate-controlled switch. In the absence of the gate control signal, the device resistance between the power terminals is large—the functional equivalence of an open switch. When the control signal is applied at the gate, the device resistance approaches zero, making the device function like a closed

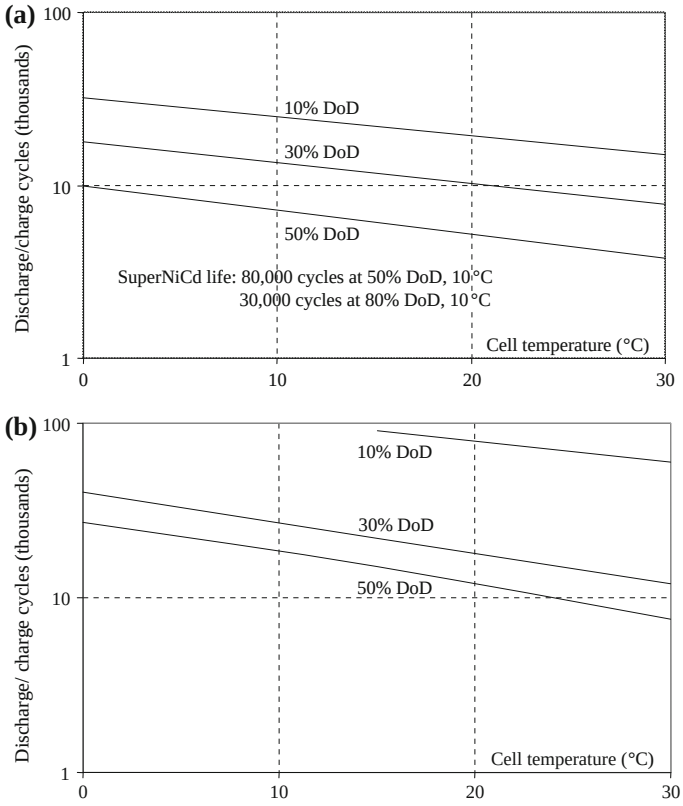

Fig. 10.12 Cycle life versus temperature and DoD for NiCd and NiH_2 batteries. **a** NiCd battery life. **b** NiH2 battery life

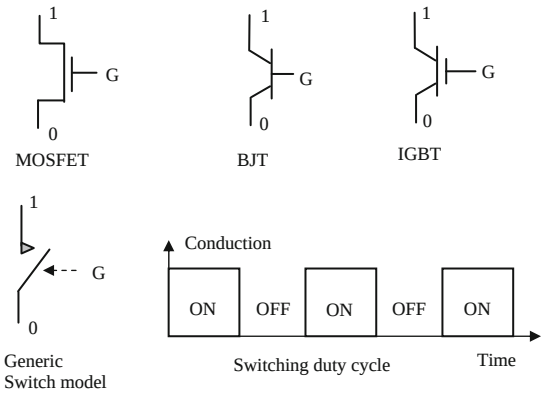

Fig. 10.13 Power electronics switching devices used in space

Table 10.4 Maximum voltage and current ratings of power electronics switching devices

Device	Voltage rating (V)	Current rating (A)	Remark
MOSFET	1,000	100	Offers higher switching speed, simpler firing circuit
BJT	1,500	200	Requires larger current signal to turn on
IGBT	1,200	100	Combines the advantages of BJT and MOSFET

switch. The current through the switching device has a maximum saturation level regardless of the voltage applied between the power terminals 1 and 0.

The switch is triggered periodically on and off by a train of gate signals of suitable frequency. Within a separate triggering (firing) circuit, a sharp rectangular signal is derived by comparing a voltage control signal with a triangular or sawtooth waveform. This on–off drive is then applied to the gate of the semiconductor switch. Although the control circuit has a distinct identity and very much different design features, it is often incorporated into the main power electronic component assembly. The transistor switch is turned on and off at high frequency, typically at 50–200 kHz, and sometimes higher. The duty ratio D of the switch is defined as $D = (time\ on/switching\ period) = (T_{on}/T) = T_{on} \times Switching\ frequency$.

The available voltage and current ratings of the switching devices and their gate triggering requirements vary with the device type. The presently available ratings are listed in Table 10.4, not all of which are space qualified. The power electronic components that use such high frequency switching devices are discussed next.

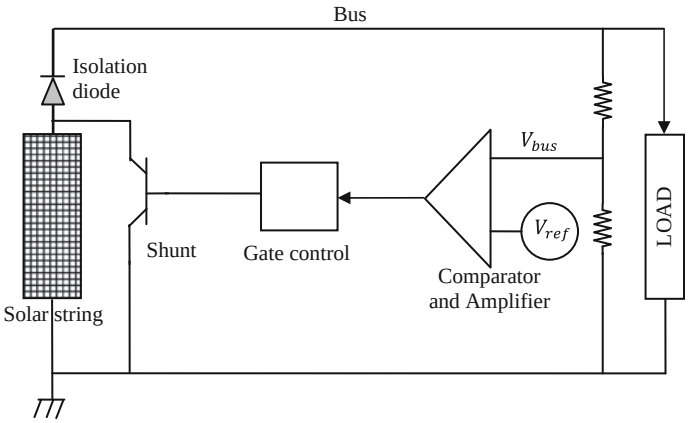

Fig. 10.14 Full shunt regulator for bus voltage control

10.2.3.2 Shunt Regulator

At the beginning of spacecraft life, the power output of the solar array during sunlight normally exceeds the load plus the battery charge requirements. The excess power must be diverted (shunted) from the bus in order to control the bus voltage. The shunt load can be a dump resistor, which would convert the solar array power into heat. Such heat dissipation in the spacecraft body would pose a burden on the thermal system in providing adequate cooling. An alternative commonly used in spacecraft is to shunt some of the solar array strings to the ground. This forces the string to operate under short circuit condition, delivering I_{sc} at zero voltage. In the shunt mode, no power is delivered to the bus or to the ground. The photon energy remains on the array, raising the array temperature and ultimately dissipating the excess power to space. The solar array is essentially being used as the thermal dissipater.

Figure 10.14 depicts a typical shunt regulator where a transistor is used as the switch. When the excess power is available, the bus voltage will rise above the rated value. This is taken as a signal to turn on the shunt switch across the required number of solar array strings. Thus, the shunt is turned on or off by a transistor controlled by the bus voltage reference. For an array with many strings in parallel, the basic configuration shown in Fig. 10.14 is used for each string separately. The same gate signal is supplied to all modules simultaneously in small power applications. For shunting large power, multiple shunt circuits are switched on and off in sequence to minimize the switching transients and the resulting electromagnetic interference to the neighboring equipment. For fine voltage control, the last shunt to turn on is operated in the pulse width modulation (PWM) mode, while all others are fully on or off.

Another application of the shunt regulator is in small satellites, where a dedicated solar array module is used to directly charge the battery without a battery charge regulator. When the battery is fully charged, the solar array module is shunted to ground by shorting the switch. This way, the battery is protected from overcharging.

10.2.4 Distribution Harness

The power distribution harness includes the insulated conductors, connectors, and the shield. Its mass is determined from the detailed layout and routing of all of the wiring required after the spacecraft has been well defined. For this reason, the harness mass is often considerably heavier than that estimated at the preliminary design stage. A typical harness mass breakdown is (1) 30 % in wires between power boxes, (2) 20 % in solar array wires, (3) 30 % in command and telemetry wires, and (4) 20 % in all connectors.

The wire size is measured in American Wire Gage (AWG) or in mm^2 cross section in metric wire gage. The AWG and Birmingham (BWG) numbers are inverse measures of the conductor's bare diameter, and are set on a log scale, i.e. AWG = 20 Log(0.325/diameter in inches). Thus, for every one gage up, the diameter increases by a factor of 1.1225 and the area by 1.26. The diameter doubles every six gages and the area doubles every three gages. The maximum current carrying capacity (ampacity) of the wire in space is less than that on the ground due to the absence of convective cooling. This requires de-rating the wire ampacity for space applications from the ground-based rating. The ampacity of various wires gages are listed in Table 10.5.

The most commonly used electrical conductor is copper for its good performance and low cost. Annealed copper has high conductivity but low tensile strength. For this reason, wires thinner than AWG 20 are often required to use high strength copper alloy 135, which has 40 % higher tensile strength, and 10 % higher electrical resistance. Copper wire coated with nickel or silver is used to resist corrosion and oxidation. Tin plated wires are widely used on the ground, but are forbidden in space due to the growth of whiskers.

Aluminum is sometimes used in power equipment where lightweight and/or low cost is desired. It is used in overhead transmission lines and pole mounted power transformers on the ground, and in some aircraft and commercial spacecraft

Table 10.5 Maximum allowable amperes in wires and connector pins of same gage

AWG[a]	Diameter (in.)	Single wire in free air on ground (MIL-STD-5088)	Wires in space[b] in 70 °C ambience (MIL-STD-975 and GSFC-PPL-19)	
			Single wire	Bundle or cable[c]
30	0.0100	n/a	1.3	0.7
26	0.0159	10.5	2.5	1.4
24	0.0201	14	3.3	2.0
20	0.0320	24	6.5	3.7
16	0.0508	37	13.0	6.5
12	0.0808	68	25.0	11.5
8	0.1285	135	44.0	23.0
4	7 × 0.0772	260	81.0	40.0
0	19 × 0.0745	460	147.0	75.0

[a] Wires sizes AWG 10, 14 and 18 are not used in aerospace for general wiring, and AWG 2 and 6 have no counterpart electrical connector contacts (pins)
[b] For TFE Teflon insulated wires rated for 200 °C
For 150 °C rated insulation, use 80 % of values shown
For 135 °C rated insulation, use 70 % of values shown
For 105 °C rated insulation, use 50 % of values shown
[c] For cable bundles of 15 or more wires in 70 °C ambience in hard vacuum. For smaller bundles, the allowable current may be proportionately increased as the bundle approaches a single conductor

Table 10.6 Copper and aluminum conductor comparison

Characteristic	Copper	Aluminum
Resistivity, Ω m at 20 °C	1.724×10^{-8}	2.830×10^{-8}
Mass density, g/cm^3	8.89	2.70
Temperature coefficient of resistance α per °C	3.93×10^{-3}	3.90×10^{-3}
Melting point, °C	1,083	660
Flex life (relative)	1	0.5
Thermal coefficient of expansion (relative)	1	1.4
Creep rate at 65 °C (relative)	1	1,000

harnesses. The performance of aluminum is compared with copper in Table 10.6. For the same power loss or voltage drop, copper can be replaced with aluminum of relative mass equal to resistivity by mass density product ratios. Aluminum conductor, therefore, would theoretically have (2.830/1.724) × (2.70/8.89) = 0.50 or 50 % of the copper mass for the same electrical performance. However, in practice, aluminum does not produce 50 % mass saving due to various mechanical reasons.

Insulation is designed to withstand the rated and abnormal transient voltages. The transient voltage can be higher by several times the rated value. The insulation design must preclude corona and arcing at pressures below 10 torr, and withstand the radiation environment and atomic oxygen. In high radiation spacecraft, such as GPS, the system specifications often require that silicon-insulated wire not be used and that the solar array wires and interconnects be welded to withstand high radiation.

A cable shield is wrapped around the wire bundle to prevent electromagnetic interference from entering the cable or radiating out. The shield can weigh 15–40 % of the cable weight. The shield options are braid versus tape, and copper versus aluminum. The braid is used when extreme flexibility is required. Its mass as compared to the wire conductor is about 40 % for flat cables and 20 % for round cables. Thin 2-mil (50 μm) copper vapor deposited on Mylar or Kapton tapes are widely used. The tape is applied on the cable with insulation touching the cable, followed by another layer on the top. The shield mass with such tapes is roughly 80 % of that with braid.

10.2.5 Solar Array Drive

The solar array drive and array drive electronics (SAD/ADE) together provide the capability of rotating the solar panels with respect to the spacecraft body. The operation of the SAD is controlled by decoded uplink commands from the on-board computer (OBC). It receives a timing clock and a synchronizing signal from the OBC. In the 3-axis stabilized 2-wing geostationary satellite, one axis is always aligned with the local normal to the Sun and another axis along the orbit normal. Two sets of open loop (clock controlled) solar array drive motors maintain the Sun orientation. A brushless DC stepper motor rotates each panel separately. The slip rings on the SAD shaft provide the interface between the rotating panel and the fixed Earth-pointing spacecraft body. One SAD controls the north panel and the other controls the south panel. The two are

interchangeable in design, where the 'forward' direction of rotation is separately selected by external means. Each SAD has only one mechanical assembly, but has redundant motor windings and redundant position telemetry potentiometers. Only one set of windings is powered at a time. The redundant windings are fully isolated to prevent failure propagation. The reliability of 0.99 is typical for both sides combined over a 15 year mission.

In an Earth orbiting satellite, the solar array is rotated once per orbit by the SAD to track the Sun at or near normal angle. The rotation is rate-servo controlled. The body information and position errors are computed by OBC to derive rate control signals. The nominal rate of rotation is mission specific and is primarily determined by the respective orbit characteristics. Using slip rings and carbon brushes is one way of providing the rotary joint between the rotating array and the satellite body. The control signals for the required rotation rate come from the telemetry, tracking and command (TT&C) system, which also selects the rotation direction. The mass of each SAD/ADE assembly can be 5–10 kg in GEO communications satellites.

The SAD/ADE provides telemetry defining its status and that of the solar panel. Each unit provides a potentiometer voltage signal which is directly proportional to the angular position of the panel shaft, ranging from 0 V at 0° to +5 V at 360°. The typical SAD uses a four-phase, 16-pole permanent magnet switched-reluctance stepper motor to drive a zero-backlash harmonic drive. Each phase coil resistance is in the 50–100 Ω range. A vanadium-cobalt steel stator core and a neodymium-iron-boron permanent magnet rotor provide high torque per unit mass. The rotor is typically on 440C stainless steel ball bearings and a titanium case. Each SAD/ADE draws power from the essential battery bus on a switchable and protected output line. The peak input power is about 10 W and the average power about 1 W. Switch-mode power pulses applied to the stator coils at a suitable frequency drive the motor. The grounding scheme for the ADE uses four separate grounds, one each for the power, signal and communications circuits, and one for all equipment chassis.

10.2.6 Electro-explosive Deployment

Electro-explosive deployment (EED) is the traditional deployment device. It is also known as pyro-technic ordnance. It uses electrical energy to ignite the squib of explosive powder. The resulting force deploys the solar array or other component, typically under a spring-loaded force. The EED will be ignited when an applied current imposes a certain amount of energy upon the squib within a specified time. For safety reasons, the squib must withstand certain minimum energy without igniting. The typical EED is rated at 1A-1 W for no fire, and 4A-4 W for sure fire.

The EED requires heavy shielding and great care with regard to the electromagnetic interference (EMI) pickup. Moreover, the EED explosive is thermal and shock sensitive. Therefore, its installation is sometimes done at the launch pad, which costs much more than at the factory. Most manufacturers install EED squibs at the factory and transport the spacecraft as class 1 explosive (sensitive to thermal and shock environment), which is also expensive.

The EED harness is routed separately from the power and signal harness in order to minimize the EMI concerns for safety. The EED technology, although used for several decades, has some disadvantages, such as (1) all spacecraft components must be designed to withstand severe pyro shock excitation, and (2) high safety related costs in documenting and reporting alerts, and complying with all other stringent regulations. The newer EMI-free alternatives are laser initiated and use shape-memory metal for deployment.

10.2.7 Design Process and Trades

Once the spacecraft-level trades are settled, the power system engineer focuses on the internal EPS-level trades that may reduce the mass and cost. The power system mass as a percentage of the satellite dry mass can range from 25 % in LEO satellites to 45 % in GEO satellites. Saving even a few percent of power system mass can result in appreciable savings at the spacecraft level. The first task of the power-system design engineer is to select the optimum primary energy source.

The bus voltage level is selected based on the power level. Early spacecraft with loads of a few hundred watts used 28 V dc, which was primarily based on the product specifications readily available for the aircraft power system at the time. Since then, the power levels have increased significantly. With power being the product of voltage and current, a high power requires a high-voltage bus in order to keep the current level at a reasonable level. Otherwise, the excessive power loss in switching devices and I^2R loss in conductors reduce the system efficiency considerably. Today's spacecraft bus voltages, somewhat standardized by the product lines of various manufactures are 28, 50, 70, and 100 V. The ISS has 160 V DC solar array voltage and 120 V DC distribution voltage [6]. The 160 V limit comes primarily from the bare conductor interaction with space plasma, particularly in LEO. Above 160 V, the solar array current leakage to plasma increases exponentially with potential sparking above 180–200 V.

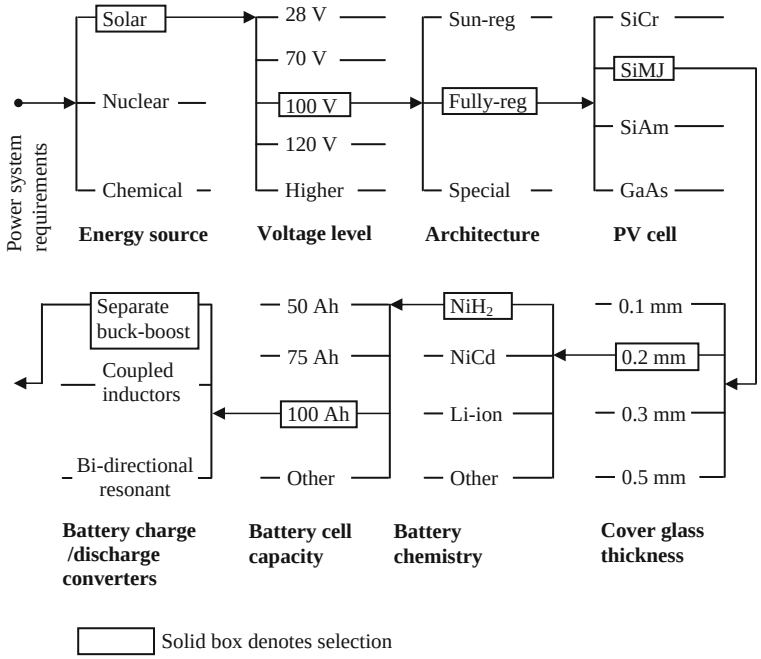

Fig. 10.15 Power system design trades flow-chart

Voltages higher than 160 V can be used in low Earth orbit with insulated cables covered in a shielded enclosure, and by encapsulating (grouting with insulating compound) all solar cell edges, connectors, and circuit board. For early space station designs [6], NASA considered 120 V dc, 270 V DC and 440 V 20-kHz ac. It finally selected 160 V DC for solar array voltage and 120 V DC for distribution bus, with necessary step-down converters for existing 28 V DC hardware. For any spacecraft, the influence factors in the voltage selections are (1) power level as the primary driver, (2) space environment and space plasma, (3) the Paschen minimum breakdown voltage between bare conductors, (4) human safety, and (5) availability of components, such as semiconductor devices, power distribution and protection devices, tantalum capacitors, etc.

Next, the power generation and energy storage technologies are jointly selected to optimize the total power system. The major driving factors are the payload power level, the operating orbit, mission life, number of satellites in the program procurement, etc. For the self-derived satellite-level load requirement, the trade study is done to select various key component for the power system, such as the PV cell, cover glass thickness for radiation protection, array substrate, battery electrochemistry and cell Ah rating, power converter topologies, etc. An example of such trades is displayed in Fig. 10.15. As the trade study proceeds from left to right, the selections made are shown by continuing arrows. Since the solar array and the battery are two components that primarily contribute to the power system mass and cost, they get more attention and see more rapid technological changes than other components. They impact not only the EPS design, but also other spacecraft systems.

10.2.8 Power System Requirements

The electrical power system requirements are seldom found in the customer specifications for the spacecraft under procurement. They are derived from the spacecraft-level requirements and in-house trade studies. The EPS self-derived requirements are based on various analyses, but the final requirements generally come from the operational orbit analyses. However, the transfer and other orbits must also be analyzed to ascertain that the proposed requirements are met in the worst case. Major self-derived requirements of the power system are (1) solar array EOL power level, (2) solar array pointing and rotation for Sun orientation, (3) battery Ah capacity, (4) battery DoD and charge control, (5) bus voltage regulation, and (6) EMI, EMC and electrostatic discharge, ESD.

The power-system design team performs the following worst-case analyses to establish detailed EPS requirements

- Power flow to determine the component ratings and heat dissipations
- Energy balance to determine the battery rating
- Voltages at the terminals of various equipment
- EOL and BOL solar array power generation capability
- Load switching and fault response, including major fuse-clearing events
- Bus stability under various feedback control loops
- Energy balance in operational and transfer orbits
- dV/dt specifications, which come from three sources
  - voltage fall after a short circuit fault until the fuse clears
  - voltage rise after the fuse clears
  - sudden loss of power during integration and testing.

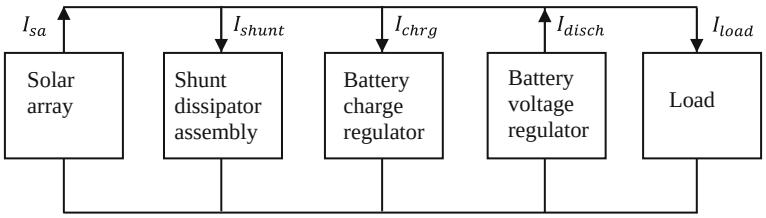

Fig. 10.16 Power system components participating in energy balance

10.3 Power System Performance

10.3.1 Energy Balance and Power Management

By designing the spacecraft electrical power system, what is really meant is designing the electrical energy system. The satellite has a limited time in orbit to generate power, but the loads need to be powered all the time. The battery stores energy during sunlight and delivers it to the loads during eclipse. The energy balance between the battery charge and discharge over one orbit period must be on average positive with some margin. Otherwise, the battery would walk to total depletion in a matter of time. The power to and from various components must therefore be managed in order to maintain the energy balance in both the transfer orbit and the operational orbit.

The energy balance analysis is performed at the design stage by simulating the power flow and energy account on a computer. The program is generally structured to allow analyses on the baseline design and its derivatives, and to answer many *what if* questions in normal and abnormal operation. Such analysis is performed during all phases of the mission for a given launch date (year, month and day). Various fault conditions, including battery cell failures (short or open) and loss of a solar array circuit, are simulated to determine energy balance under the worst-case condition(s). Other equally important uses of the energy balance computer program are

- Determine and/or optimize the load capability of a given EPS
- Derive component ratings based on maximum power flow in each component
- Determine power dissipation for thermal design of each component, particularly the battery, since its performance is highly temperature sensitive.

The computer program for such analysis is generally developed around variable parameters with no *hard-coded* numbers. This allows greater flexibility in using the tool for a wide variety of applications. Figure 10.16 depicts EPS components contributing to the energy balance program. The basic equations for currents and battery DoD that are computed typically every second or so in the energy balance analysis are

$$During\ sunlight,\ I_{sa} = I_{load} + I_{chrg} + I_{shunt} - I_{disch} \quad (10.6)$$

$$During\ eclipse,\ I_{load} = I_{disch} \quad (10.7)$$

$$DoD(t) = DoD_0 + (Sum\ of\ Ah\ delivered/\text{Actual Ah capacity}) \quad (10.8)$$

where DoD_0 is the initial DoD.

The entire program is divided into several software modules, each representing various components. Due to the non-linear nature of the battery cell and solar array performance parameters, the program typically uses *static* lookup tables to determine the cell performance characteristics as a multi-variable function of the battery current, temperature, state of charge, and the solar array operating voltage. Programming with a computer language, instead of modeling on a spreadsheet, significantly improves the capability of the program.

10.3.1.1 Dynamic Performance and Stability

The dynamic bus impedance and the control loop gain influence the dynamic performance of the power system under an internal or external transient perturbation. Key performance attributes coming out of the dynamic study are the bus voltage ripples, transient deviations, fault and fuse-clearing transients, and the control loop stability under harmonic ripple excitation. On the other hand, the static performance under a slow change or after the dynamic response has settled, is largely influenced by the static impedance of the bus. The bus voltage change long after a load change is an example of static performance. Since the dynamic and static bus impedances are similarly defined, they are jointly covered in the following section.

10.3.1.2 Bus Impedance

A complex electrical network having a number of sources and loads between any two terminals can always be reduced to a simple Thevenin equivalent source model consisting of one source voltage V_s with an internal series impedance

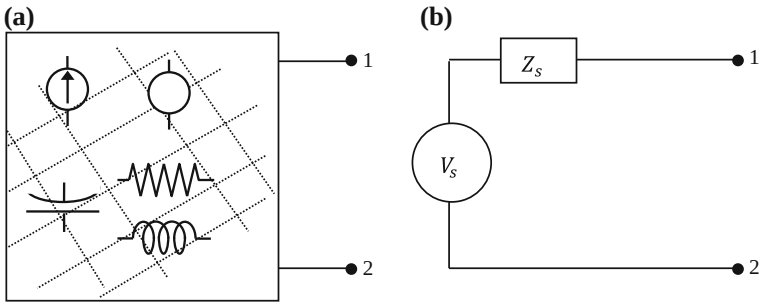

Fig. 10.17 Thevenin equivalent source model of complex electrical network. **a** Complex electrical network. **b** Thevenin equivalent source

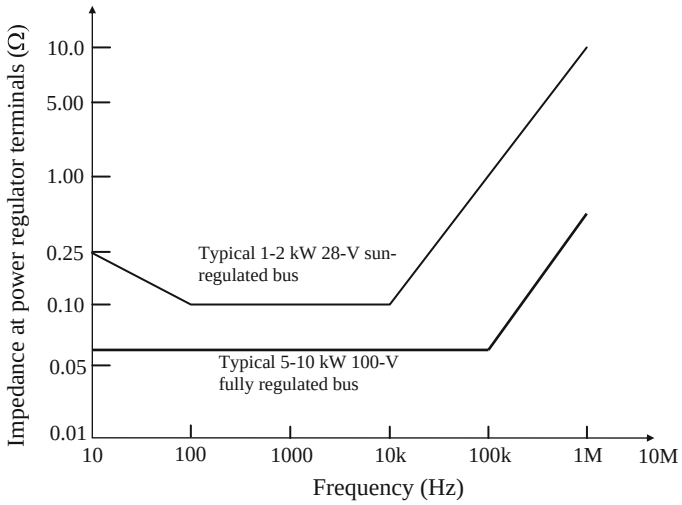

Fig. 10.18 Main bus source impedance for a 28 and 100 V GEO communications satellite

Z_s (Fig. 10.17). The two source parameters are determined as follows

- With open circuit between load points 1 and 2 as in Fig. 10.17b, but with all other parameters at rated values, the voltage between terminals 1 and 2 equals the source voltage V_s (since the internal voltage drop is zero under zero load current). Therefore, V_s is the open circuit voltage of the system at the load terminals.
- With the terminals 1 and 2 shorted, the internal voltage is now totally consumed in driving the current through the source impedance only. Therefore, Z_s is the open circuit voltage/short circuit current at the load terminals.

The short circuit current can be determined by calculations, or by tests at a reduced voltage applied to limit the current to the rated value. The full short circuit current is then calculated by scaling to full rated voltage. Any non-linearity, if present, must be accounted for. The source impedance of most spacecraft bus architectures is highly non-linear due to use of multiple bus regulators along with dead-band regions. The dynamic performance of such systems is largely driven by the transient nature of switching from one mode to another, such as solar array shunt control to battery discharge control. Linear modeling may be acceptable for steady-state regulation and small signal load changes within the control range of each controller, but not for modeling mode change transition, which must use a transient model for the individual control.

The Thevenin equivalent source model derived under the steady-state static condition gives the static bus impedance Z_s. The source impedance derived under the dynamic condition (that is for an alternating or incremental load) is the dynamic bus impedance Z_d. This varies with frequency and can be either calculated or measured by test. With the bus in operational mode delivering its rated load, a small high frequency AC current I_h is injected into the bus using an independent current source, and the value of V_h, the high frequency voltage perturbation in the bus voltage, is measured. The dynamic bus impedance at that frequency is then $Z_d = (V_h/I_h)$. Since Z_d has a strong influence on the system's dynamic performance, it is kept below specified limits. Figure 10.18 is a typical main bus source impedance for a mid-size GEO communications satellite.

10.3.1.3 Stability Criteria

The steady-state stable operating point is where a PV panel's power output equals the load power. The constant power load has two such points, A_1 and A_2 shown in Fig. 10.6. If point A_1 gets a small disturbance of $+\Delta V$ for any reason, there would be a positive power excess, moving the voltage higher from A_1, and again further higher in a runaway

situation. On the other hand, at point A_2, a small voltage disturbance of +ΔV due to any reason would result in a power deficit, restoring the system back to its original operating point A_2. Thus, point A_2 is a stable operating point, where the system works like a negative feedback system. Analytically, an operating point is stable if and only if

$$\left[\frac{dV}{dI}\right]_{source} < \left[\frac{dV}{dI}\right]_{load}. \tag{10.9}$$

In terms of the absolute values of the dynamic impedances, Z_s is the source output impedance and Z_L is the load input impedance, the system is stable only if $Z_s < Z_L$ at all frequencies. When $Z_s > Z_L$, the system is not necessarily unstable and requires further analysis to determine the stability. The constant power load gives a stable operating point only on the right-hand side of the P_{max} point. The solar array powering a purely resistive load is always stable, since Eq. 10.9 is always true.

10.3.2 Electromagnetic Interference, Compatibility and Electrostatic Discharge

All spacecraft systems are required to be compatible with the interference expected from internal and external sources. For decades, the electromagnetic interference (EMI) and electromagnetic compatibility (EMC) requirements have come from MIL-STD-461. It specified the maximum emission limit of the potential culprit, and the minimum susceptibility level of the potential victim equipment. The companion MIL-STD-462 defined the test methods for verifying that MIL-STD-461 requirements were met, and MIL-STD-463 defined the applicable terms and units. The first two standards are now merged into one, MIL-STD-461. The contractor of commercial and defense spacecraft is required to develop three documents and submit to the customer as deliverables: (1) EMC control plan, (2) EMI test plan, and (3) EMI test report.

10.3.2.1 EMI Sources and Suppression

The EMI requirements broadly fall in two general groups, the conducted EMI and the radiated EMI. In fact, EMI can enter the equipment either by conduction via wires, or by radiation in space. In verifying that a spacecraft will meet these requirements, the first order of task is to determine the conducted EMI and the radiated EMI from potential sources, and the degree of coupling to the victim equipment. In space systems, the main sources of EMI are (1) switching large current or voltage at high frequency causing large (dI/dt) and (dV/dt), (2) electrostatic discharge, and (3) nuclear detonation around the spacecraft. Various methods of controlling and/or suppressing the EMI in the spacecraft are, in the order of their importance

- Minimize the EMI generation in the first place by
- Minimizing the current loop area in switching circuits
- Minimizing the switching transient's (dI/dt) rate in large current loops
- Using snubber capacitors to minimize the voltage transient's (dV/dt) rate
- Minimize the E and B field couplings between the culprit and the victim equipment by
  - Minimizing the inductive coupling by twisting wires or using coax cables
  - Minimizing the capacitive coupling by using shields and by reducing area of exposed metal and keeping it far from the ground, since $C = (kA/d)$.
- Divert the energy impinging on the victim equipment to ground by using
  - Proper grounding scheme
  - Faraday shield, single or double.
- Protect the equipment from the coupled energy by using
  - L-C filters for conducted EMI.Enclosure shield for radiated EMI.

10.3.2.2 Electrostatic Discharge

An electrostatic charge accumulates on any probe in space regardless of its being in or out of the van Allen belts. The accumulated charge raises the electrical potential of the probe, causing a current flow from the probe to the surrounding plasma. If the current cannot maintain a balance of charge, the probe's potential will keep rising until arcing takes place. This problem can occur particularly when the spacecraft leaves or enters an eclipse, when the interaction with space suddenly changes. Arcing can also arise due to differential charging of insulated surfaces that are not electrically connected. Each isolated surface acts as an independent probe in space, which eventually floats to a potential that results in no net current to or from the space plasma. That potential is of the order of the plasma kinetic energy. Insulating surface do not distribute surface charge, hence can charge up to much higher differential potential until discharge takes place by way of arcing and/or flashover.

The charging, the subsequent electrostatic discharge (ESD), and their remediation in GEO and in LEO are significantly different. In the high-energy plasma environment of GEO, the electron charge that accumulates on insulating surfaces increases the electric field to adjacent conductors above the breakdown level, leading to arcing. The resultant arcing currents traveling through conductors can upset electronic components and induce spurious signals. A common design solution for GEO is to coat all outside surfaces of the spacecraft with conducting materials. This prevents differential charging by distributing the charge over all

surfaces and equalizing their potentials. A coating material having surface sheet resistivity of less than 5 kΩ/sq[1] is considered adequate to eliminate differential charging. On solar arrays, indium oxide type conductive and transparent coating is applied on the cover glass when required.

In LEO, because of the high thermal plasma current density, surfaces do not ordinarily collect much differential charge. The major concern in LEO is the absolute charging of spacecraft surfaces with respect to the surrounding plasma. Normally, the collected plasma current bleeds off the absolute potential rapidly.

10.3.3 De-rating Parts for Reliability

The U.S. Military Handbook-217 (MIL-HDBK-217) establishes the uniform method of predicting the reliability of military electrical and electronic parts, equipment, and systems. It lists the base failure rates per million hours of operation for numerous parts under base electrical, thermal, and mechanical stresses. Any deviations from the specified operating conditions would alter the failure rate listed in the handbook.

The failure rate of an electrical component depends primarily on voltage and temperature. The electrical insulation at high temperature oxidizes, becomes brittle, and may crack, leading to failure (short circuit). The oxidation is a chemical degradation, and follows Arrhenius exponential growth. Data from a range of electrical equipment shows that the failure rate doubles (or the life is shortened to one-half) for every 7–10 °C rise in the operating temperature. In the reverse, the life doubles for every 7–10 °C reduction in the operating temperature. Similar degradation (wear) takes place above a certain voltage, although it is not as well understood as that for the temperature. The rise in failure rate at high stress level is not to be confused with the wear-out failure rate. It raises the flat part of the classical bathtub curve for reliability. The failure rate is still constant per unit time, although another constant at another operating stress level.

De-rating is the reduction of electrical, thermal, and mechanical stress levels applied to a part in order to decrease the degradation rate and prolong the expected life. It is routine practice to decrease the wear-out failure rates in military and space worthy designs. The de-rating in current is often done to lower the temperature. On the other hand, the current de-rating in some active devices, such as transistors, is done to control the (dI/dt) rate, which can upset the semiconductor operation; de-rating increases the margin of safety between the operating stress level and the actual failure level of the part. It provides added protection from system anomalies unforeseen by the design engineer.

Most space programs maintain their own preferred parts list based on the failure rates. This preferred parts list also gives de-rating factors, which must be applied to all designs on those programs. Both the selections of parts and the de-rating factors in the preferred parts list are based on the heritage designs successfully flown. Space agencies, such as NASA and ESA, maintain their own preferred parts list. If a desired component is not in the preferred parts list, it must be qualified by rigorous testing under the same environment as those in the list.

10.4 Special Power Systems

10.4.1 Interplanetary Mission

The mission environment depends heavily on the spacecraft's distance from the Sun. For interplanetary missions away from the Earth—either, closer to the Sun or farther away from the Sun—the solar array, battery, and power electronics designs differ significantly because of the significantly different environment encountered. The extreme temperature on either side—high or low—has a large impact on the performance. The solar flux at any distance in deep space is given by $I = (I_{earth}/R^2)$, where I_{earth} is the solar flux in the Earth's orbit, and R is the distance from the Sun in astronomical units (au). This equation assumes the Sun to be a point source, and may give some error at distances less than a few solar radii. The solar array power output varies linearly with the incident solar flux. Therefore, as the spacecraft moves away from the Sun, the power decreases inversely with the distance squared. The PV array temperature also decreases in the same ratio, which results in a higher PV conversion efficiency. The combined effect of the flux and the temperature changes is such that the photovoltaic power generation varies not inversely with the distance squared, but with R^{α}, where α is approximately 1.5. Table 10.7 lists planets in our solar system with their distances from the Sun in au, and approximate power generation rate in their orbits, considering both the solar flux and the temperature variations. See also Table 4.3.

Due to the Sun's proximity, the electrical power system for a Mercury mission must meet the harsh thermal and radiation environment. Haines [7] of the European Space Agency has reported the power system design for a Mercury

[1] Sheet Resistance is a special case of resistivity for a sheet of uniform thickness. The SI unit if resistivity is ohm · meter (Ω · m), which is more completely stated in units of Ω · m^2/m (Ω · Area/Length). When divided by the sheet thickness, 1/m, the units are Ω · (m^2/m^2) = Ω. The alternate, common unit is 'ohms per square' (denoted 'Ω/sq'), is dimensionally equal to an ohm and exclusively used for sheet resistance avoiding misinterpreted as bulk resistance of 1 Ω. Note that a square sheet with sheet resistance 50 Ω/sq has an actual resistance of 50 Ω independent of the size of the square.

Table 10.7 Solar flux and PV power generation in orbits of various planets in our solar system (relative to those in the Earth's orbit)

Planet	Distance from the Sun (au)	Solar flux relative to Earth orbits	PV power generation accounting for temperature difference
Mercury	0.31–0.47	10.40–4.52	Severe loss of voltage
Venus	0.72	1.93	1.63
Earth	1.0	1.0	1.0
Moon	1.0	1.0	1.0
Mars	1.66	0.36	0.59
Jupiter	5.20	0.037	0.084
Saturn	10.08	0.0098	0.031

sample return mission. It consists of three independent power systems for each phase of the mission. For example, the 20 kW, 100 V high-power system shown in Fig. 10.19 is used for electric propulsion, and is jettisoned just before the orbit insertion. After that, the 500 W, 28 V system is used for the orbiter, and a smaller power system for the surface landing, sample collection, and return phase of the mission.

10.4.2 Near-Sun Mission

The PV power system design for near-Sun missions between Mercury and the Sun needs special considerations due to the high temperature. The solar intensity increases to 100 Suns at 0.1 au (21 Sun radii, 1 Sun radius equals 0.00476 au), and to 2,500 Suns at 0.02 au (about 4 Sun radii). The PV cell loses power generation capability at such temperature due to loss in the open circuit voltage. Various options to limit the temperature to below 1,000 °C include reliably guaranteed array tilting, adding mirrors on the surface to decrease absorptivity and increase emissivity, partially silvered cover glass, and various louvers and shades to control the solar flux. Moreover, the PV cell having high band gap is needed. Figure 10.20 due to Brandhorst and Chen [8] shows effective power output as function of au distance and band gap of various PV cells operating below 1,000 °C. At distance greater than 0.5 au, the band gap has no significant effect on power generation. At distance less than 0.5 au, the higher band gap PV cell generates more power up to 0.1 au. Closer than 0.1 au, the PV cell becomes useless. The curves assume that the cell temperature is limited to 1,000 °C in all cases.

It is apparent from Fig. 10.20 that the PV power system has limitations in approaching the Sun at a close distance. An alternative approach may be to use the thermo-photovoltaic (TPV) direct energy conversion. There are several advantages, including easy coupling to a thermal source operating above 2,000 K. The feasibility of such an approach has been demonstrated under US Department of Energy funding, but not fully developed.

Another alternative is to use a thermoelectric (TE) converter with the Sun as the heat source. Such a system is feasible for solar probes requiring instrument power under a few hundred watts. For example, NASA/JPL in 2003 designed the Sun-TE power system for a flyby probe to Jupiter and then towards the Sun to study coronal heating and the origin and acceleration of the solar wind. In the power system design reported by Choi [9], the probe's distance from the Sun varies greatly, from 5.2 au near Jupiter (gravity assist orbit) to less than 0.1 au (4 solar radii) near the Sun. The corresponding solar flux varies over 5 orders of magnitude from 50 W/m^2 to 4 × 10^6 W/m^2. The spacecraft bus is shaded by the primary sunshield blocking the Sun. The shield's outside temperature is estimated to be 2,100 °C at 4 solar radii. A high temperature multi-layer thermal blanket keeps the spacecraft components cool. The shield and the blanket are made of carbon–carbon composite.

10.4.3 Deep Space Mission

Deep space and outer planetary missions cannot effectively use photovoltaic power generation due to insufficient solar flux. For those missions, an on-board radioactive isotope is often used to generate electrical power. The radioisotope heat is directed at a TE junction, which generates electrical potential just as in a thermocouple. The power system for such missions, therefore, typically includes a radioisotope thermoelectric generator (RTG), power electronics, and a small battery located inside the spacecraft body. The RTG heat may be sufficient to protect the power system from cold temperatures. If not, an additional isotope heat is needed to keep the electronics at required temperature. For example, unheated interplanetary spacecraft launched to explore the rings of Saturn would experience an average temperature of about −190 °C, which is the temperature of liquid nitrogen. For this reason, low temperature power electronic circuits have potential of finding applications in deep space missions. Such circuits designed and operated at low-temperature may result in more efficient system layout than the room temperature circuits. The advantages include reducing or eliminating the thermal shutters and the need for an isotope heat, which can cause overheating during launch. Understanding the performance of power electronics at extreme low temperatures is needed for this purpose. The following is known about the operation of power electronic components near the liquid nitrogen temperature.

Performance of certain semiconductor devices improves with decreasing temperature down to liquid nitrogen

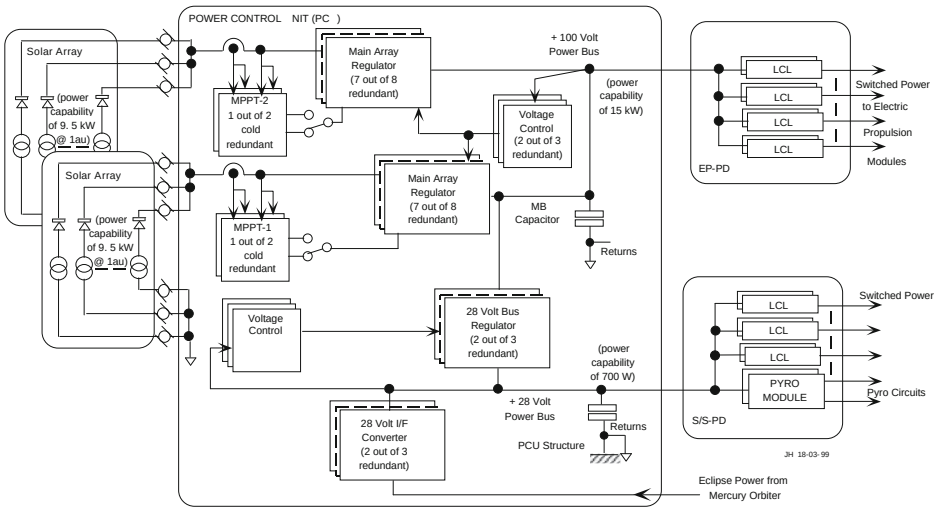

Fig. 10.19 Main bus power system architecture for electric propulsion to Mercury. *Image* J.E. Haines, ESA

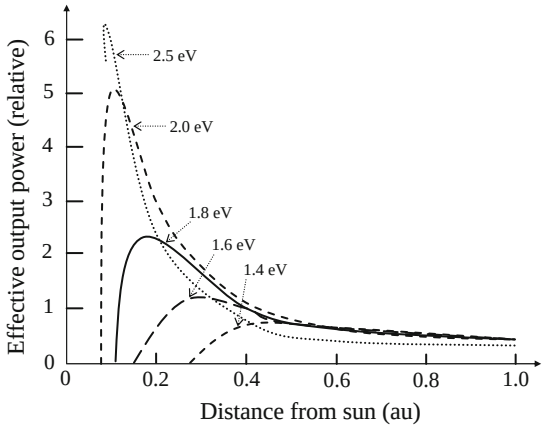

Fig. 10.20 Power output versus distance for PV cell of various band gaps at temperature below 1,000 °C

temperature. At low temperatures, majority carrier devices demonstrate reduced leakage current and reduced latch-up susceptibility. In addition, these devices show higher operating speed resulting from increased carrier mobility and saturation velocity. An example is the power MOSFET, which has lower conduction loss at low temperatures due to the reduction in drain-to-source resistance $R_{ds(on)}$ resulting from increased carrier mobility. NASA has tested other components such as resistors, capacitors, and magnetics that are needed for various power converters at liquid nitrogen operating temperature. Many of them have been found suitable for operating an unheated interplanetary spacecraft [10].

The battery can be a roadblock at very low temperatures. The Li-ion battery offers a somewhat favorable combination of energy and power density. However, its low temperature performance below −40 °C is poor. Tests have shown the following about the Li-ion cells [11, 12]

- Between room temperature and −20 °C, variations in electrolyte resistance and the anode to electrolyte resistance are negligible, but the cathode electrolyte interface resistance increases substantially.
- The cell voltage and Ah capacity fall to approximately one-half at −40 °C. As a result, practically no energy was delivered at −40 °C. This is due to substantial increase in the total internal resistance.
- Poor cell performance at low temperatures can be attributed to the electrolyte becoming viscous or solid [13]. It is also attributed to the poor lithium diffusivity in the electrolyte. Work is underway to improve the low temperature performance of the Li-ion cell.

10.4.4 Radioisotope Thermoelectric Generator

An RTG for power levels of several hundred watts has been fully developed and used for decades. Such a power source has the advantage of supplying power all the times, thus eliminating the need for a battery in a base load system having no peak power requirement. An obvious disadvantage is the heavy radiation shielding required around the electronic components. The advantages of the RTG are

- It provides power for a long period, independent of the spacecraft orientation and distance from the Sun.
- It is suitable for missions far away from the Sun, too close to the Sun, or lunar missions with long eclipse periods.
- The power output is not affected by radiation damage in the Van Allen belts or from man-made nuclear threats.

The RTG consists of numerous thermoelectric cells connected in series–parallel combination to obtain the required voltage and current. Each TE cell converts the isotope thermal energy into electrical energy. The power conversion efficiency of the RTG depends on the material properties and the hot and cold junction temperatures T_{hot}

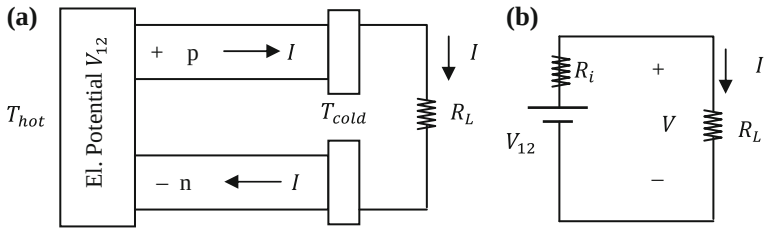

Fig. 10.21 Single-stage unicouple thermoelectric junction. **a** Construction **b** Electrical model

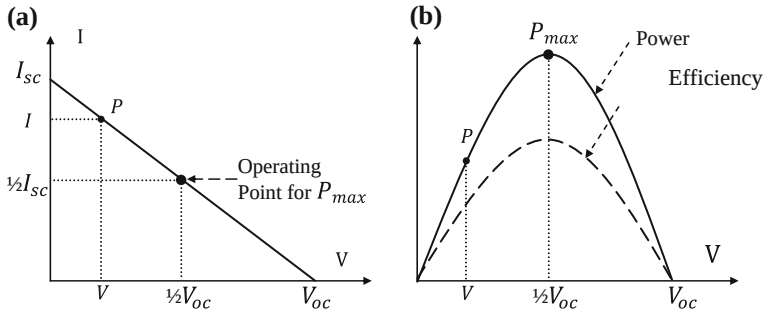

Fig. 10.22 Thermoelectric I–V and P–V curves with P_{max} point. **a** I–V characteristic. **b** P–V characteristic

and T_{cold}. The theoretical limit on this efficiency is Carnot cycle efficiency, $\eta_{carnot} = [(T_{hot} - T_{cold})/T_{hot}]$, where the temperatures are on the absolute Kelvin temperature scale. Practical designs yield about one-half the theoretical maximum efficiency. The most widely used material (Plutonium-238, ^{238}Pu isotope with SiGe TE cells) gives about 7 % conversion efficiency. Removing the remaining 93 % of the system energy as waste heat poses a significant design challenge. The specific electrical power output of RTG is typically low. Based on the total power system mass, it was 5 W/kg in the Galileo spacecraft. The ^{238}Pu isotope is also scarce and expensive, a few million dollars per kilogram. The US did not produce it for some time, instead purchasing it from Russia, with the US Department of Energy inventory of ^{238}Pu dropping below 10 kg, however US production of ^{238}Pu recommenced in 2013/14.

10.4.4.1 Thermoelectric Basics

The working principle of a TE converter is based on the Seebeck effect, which generates electrical potential when any two dissimilar materials are maintained at different temperatures. It involves electron or hole transfer between two dissimilar materials under thermal energy. The two materials can be conductors or semiconductors. The TE cells for space power applications use semiconducting materials, one p-type and the other n-type, as shown in Fig. 10.21. If two such dissimilar materials are held at a temperature difference $\Delta T = (T_{hot} - T_{cold})$, an electric potential difference V_{12} is produced at their junction. It is given by $V_{12} = (\alpha_{12}\Delta T)$, where α_{12} is known as the Seebeck coefficient of the couple, generally expressed in μV/°C. The coefficient α_{12} is often called the TE power, although it is not really a power. It is a characteristic constant, which depends on the material properties. The α_{12} is considered positive if the Seebeck voltage polarity produces current in the p-type material from high temperature to low temperature.

The total voltage generated due to the Seebeck effect works as an internal voltage source. With open circuit (zero load current), the external terminal voltage V is same as V_{12} generated internally. This voltage is designated as the open circuit voltage V_{oc}. When electrical current is drawn by load resistances R_L, there is an internal voltage drop. This is represented by an internal resistance R_i, which is approximately constant at a given temperature. The external terminal voltage V therefore decreases linearly with increasing load current, i.e. $V = (V_{oc} - IR_i)$. With the external terminals shorted, the maximum current flows to the load. This current is designated as I_{sc}, which is given by $I_{sc} = (V_{oc}/R_i)$. These equations can be rearranged to write $I = (I_{sc} - \gamma V)$, where $\gamma = (I_{sc}/V_{oc})$, the characteristic admittance of the RTG power source. The last equation in this paragraph gives the I–V characteristic of the RTG. It is a falling straight line from I_{sc} at zero voltage to zero current at V_{oc} as shown in Fig. 10.22a.

10.4.4.2 Maximum Power Extraction

The power transferred from the RTG to the load at any operating voltage V and load current I is $P = VI = V(I_{sc} - \gamma V) = (VI_{sc} - \gamma V^2)$. The power system design for

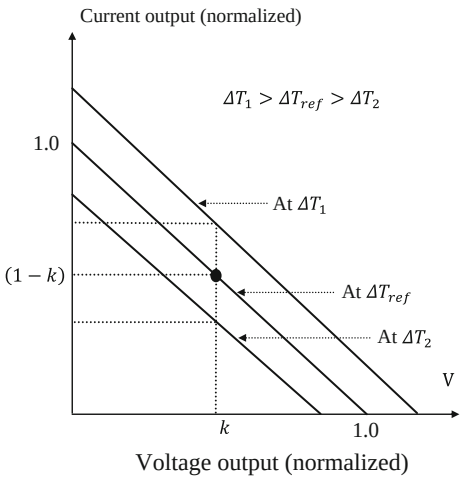

Fig. 10.23 Thermoelectric current versus voltage and various temperature gradients

extracting the maximum power from the RTG to the load must operate at a voltage such that $dP/dV = I_{sc} - 2\gamma V = 0$ at the operating voltage. This equation gives the corresponding operating voltage $V_m = I_{sc}/(2\gamma)$, which is also 1/2 V_{oc}, and the current at that voltage is 1/2 I_{sc}. The maximum possible power transfer from the RTG to the load is therefore

$$P_{max} = \frac{V_{oc}}{2}\frac{I_{sc}}{2} = \frac{V_{oc}I_{sc}}{4}. \qquad (10.10)$$

P_{max} occurs when the RTG is operated at a voltage equal to one-half of the open circuit voltage, as shown in Fig. 10.22b. The power at zero voltage is obviously zero. It is also zero at V_{oc} since the current is zero there. In between, the power rises with the operating voltage, reaches the maximum value P_{max}, and then falls to 0 at V_{oc}. The RTG conversion efficiency is maximum at the maximum power transfer point.

10.4.4.3 Effect of Temperature and Aging

The I–V line of the RTG shifts upward for a higher ΔT, and downward for a lower ΔT, as shown in Fig. 10.23. The amount of shift is a characteristic of the couple material. Aging has a small effect on the RTG output, because the basic heat source has a long half-life in decades. For this reason, the power generation degrades a little, about 1.5 % per year (Fig. 10.24). Most power degradation is due to slow precipitation of the phosphorous doping in the n-type leg of the thermocouple. The I–V and P–V curves shift uniformly with time and temperature such that the maximum power point remains at the same voltage. This is a happy coincidence for the design engineer. The conversion efficiency is a function of the contact resistance and the hot and cold-side temperatures.

10.4.5 Dynamic System with Alternator

Solar energy can be used in a system other than photovoltaic. A dynamic energy conversion system is an example, where the Sun's energy is collected in the form of heat using a concentrator. The heat in turn is used to produce steam and drive a rotating turbo-generator or a reciprocating alternator to generate electrical power. Such a system was a primary candidate for the space station design in the 1980s for a power requirement of 300 kW. The system configuration is shown in Fig. 10.25. A parabolic concentrator focuses the Sun's heat on a receiver, which boils a fluid. The fluid can be a suitable liquid metal, such as potassium chloride. High-pressure steam of liquid metal produced in the receiver drives a turbine based on a Rankin cycle. The fluid can also be a gas, such as a mixture of helium or xenon having a molecular weight of around 40. The heated compressed gas in this case drives a turbine working on a Brayton cycle. A gas-based system minimizes erosion and sloshing problems in transporting the liquid metal. In either a liquid metal or a gas-based system, the high-pressure high-temperature fluid drives the turbine, which in turn drives an electrical generator. Waste heat transferred to the liquid coolant is dissipated via radiator panels to space. The energy conversion efficiency is much higher than the photovoltaic system. This minimizes the deployed collector area and the aerodynamic drag of LEO.

The usable energy extracted during the thermodynamic cycle depends on the working temperatures. The maximum thermodynamic conversion efficiency that can be theoretically achieved is Carnot cycle efficiency. Higher hot-side working temperature and lower cold-side exhaust temperature results in higher efficiency of converting the captured solar energy into electricity. The hot-side temperature however, is limited by properties of the working medium. The cold-side temperature is largely determined by the cooling method and the environment available to dissipate the exhaust heat. An indirect but major advantage of this system is that the energy storage is interwoven in the system at no extra cost. It resides in the latent heat of phase change at a high temperature of around 1,000 K. The system can store thermal energy for hours with no electrical performance degradation, or longer with some degradation. This feature makes this technology capable of meeting peak power demands with no added mass or cost of separate energy storage. It eliminates the battery requirement altogether.

Although the solar dynamic technology is not yet proven in space, it offers potential advantages in efficiency, weight, scalability, and the overall cost in high-power spacecraft. The cost advantage comes from the elimination of costly semiconductor PV cells. Such a system can be cost effective in a

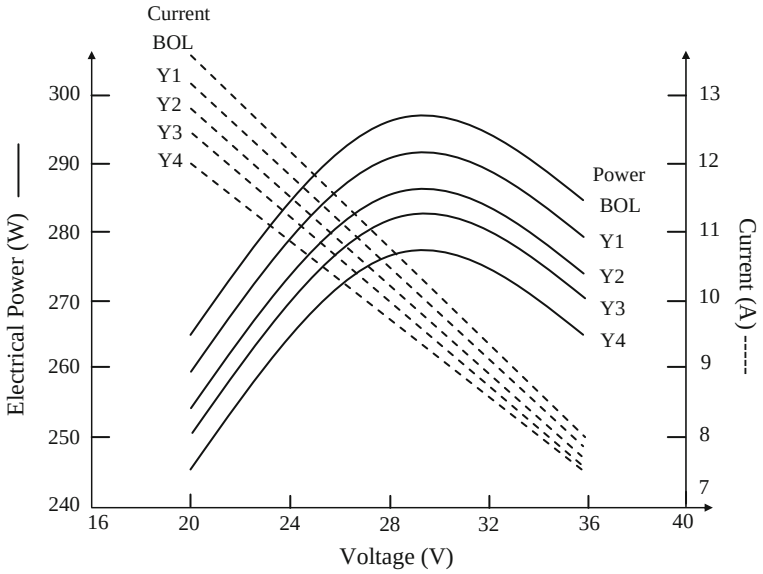

Fig. 10.24 RTG I–V–P characteristics of RTGs at various operating age in years

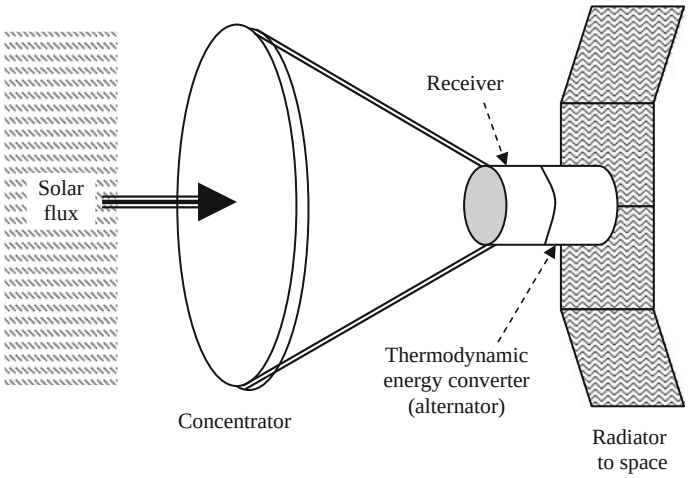

Fig. 10.25 Solar concentrator with dynamic alternator

few kilowatts to hundreds of kilowatts power range. The concept is sufficiently developed for space use in the near future, particularly in high-power LEO missions. It may also find applications in high-power defense spacecraft where large solar arrays can make the vehicle non-maneuverable and vulnerable to the detection and attack by enemy. It has been considered in the past for a 300 kW space station and for a dynamic isotopes power system (DIPS) for space defense.

The efficiency advantage in the dynamic system comes from the higher efficiency of the engine (25–40 %) as compared to silicon solar cells (15–25 %), and higher efficiency of thermal energy storage of the receiver (85–90 %) as compared to the battery efficiency (70–75 %). The greatly improved overall system efficiency as compared to the PV system translates into less solar collection area. This results in reduced drag and relaxed concern regarding station dynamics, approach corridors, and experiment viewing angles. The reduced drag is particularly important because it allows lower flight altitudes within given constraints of drag-makeup fuel and orbit decay time. At power levels near 100 kW, such as for space-based radar, the PV solar array collector area becomes prohibitive. The solar dynamic power system is expected to find advantageous applications in this power range.

Recent prototype testing of a 2 kW non-optimized solar dynamic systems reported by Mason [14] demonstrated a conversion efficiency of 30 % using 1990s component technologies. Significant improvements in efficiency can be realized for large systems with ratings above 100 kW using newer technology components and optimized design parameters.

10.4.6 Fuel Cell Power

The fuel cell was developed as an intermediate-term power source for space applications. It was first flown on the Gemini V crewed mission in 1965. It has been routinely

used to power NASA's fleet of Space Shuttles that carried components and crew to the International Space Station and other space service missions [15]. The fuel cell resembles a battery in that it converts the chemical energy of a fuel directly into DC electricity. However, unlike a battery, it does not run down in energy and does not have to be recharged. It keeps producing electricity as long as the fuel is supplied. The typical fuel gas is hydrogen or a hydrogen-rich mixture and an oxidant. One pound (450 g) of hydrogen has 52,000 Btu or 15.24 kWh primary energy and requires 8 pounds (<3,600 kg) of oxygen to react.

The fuel cell finds applications in space missions lasting for a few days to a few weeks where the battery is not practical. It also has a potential use as auxiliary power source for orbit transfer vehicles. The regenerative fuel cell integrated with an electrolyzer unit presents an attractive mass saving for LEO satellites requiring large energy storage. It was a candidate in place of the battery for the ISS.

The working of the fuel cell is the reverse of electrolysis. In electrolysis, electricity is injected between two electrodes in water to produced hydrogen and oxygen. In the fuel cell, hydrogen and oxygen are combined to produce electricity and water. The energy conversion is direct from chemical-to-electrical. Since the process is isothermal, the conversion efficiency is not limited by Carnot efficiency. This is unlike chemical-to-thermal-to-mechanical-to-electrical energy converters using steam or an internal combustion engine. It skips the usual combustion step of the conventional thermodynamic power system and converts a high percentage of the fuel's available free chemical energy directly into electricity. The fuel cell efficiency, therefore, can be about twice that of the thermodynamic converter. It is as high as 65 % in some designs, and 75–80 % in solid metal oxide fuel cells developed for ground-base power plants. Its superior reliability with no moving parts is an additional benefit over the thermodynamic power generators.

10.4.6.1 Electrochemistry of Fuel Cell

The fuel cell consists of anode and cathode electrodes separated by a liquid or solid electrolyte. The electrodes are electrically connected through an external load circuit as shown in Fig. 10.26. Hydrogen or a hydrogen-rich mixture is fed to the anode. The hydrogen fuel is combined with oxygen of the oxidant entering from the cathode port. The hydrogen, however, does not burn as in the internal combustion engine. It splits into hydrogen ions (H^+) and electrons (e^-), and produces electricity by an electrochemical reaction. Water and heat are the byproducts of this reaction if the fuel is pure hydrogen. With natural gas (ethanol or methanol) as the source of hydrogen—as in some ground-based fuel cells—the byproducts include carbon dioxide and negligible traces of carbon monoxide, hydrocarbons, and nitrogen oxides.

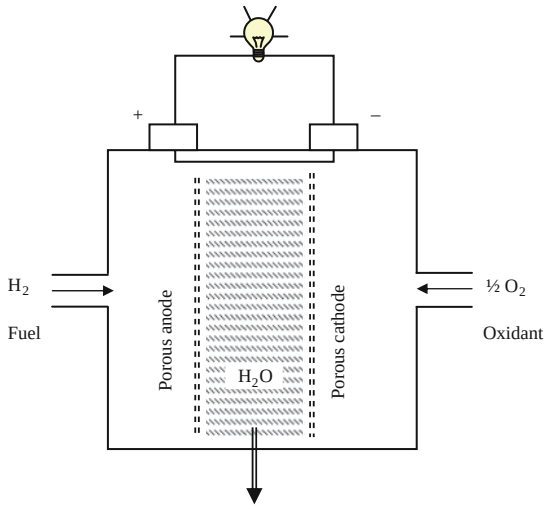

Fig. 10.26 Fuel cell construction and operation

The hydrogen–oxygen fuel cell consumes hydrogen as fuel, oxygen as oxidant, and an aqueous acid solution as electrolyte. Their net reaction is $2H_2 + O_2 = 2\,H_2O$, and of course energy is released in the process. In one type of fuel cell, the electrons flow from the anode and travel through the external circuit to the cathode, powering the electrical load connected to the terminal. The hydrogen ions migrate through the electrolyte to the cathode, closing the loop. At the cathode, they combine with the oxygen and the incoming electrons from the external circuit to produce water. The kind of ions and the direction in which they migrate varies, depending on the type of electrolyte.

The fuel cell is thus a static electrochemical device that generates electricity by chemical reaction without altering the electrodes or the electrolyte materials. This distinguishes the fuel cell from the electrochemical battery. Unlike the conventional battery, the fuel cell has no electrical energy storage capacity. Hence, it must continuously supply the reactant and withdraw the reaction products during operation.

10.4.6.2 Fuel Cell Performance

The fuel cell works as a voltage source with an internal resistance. The electrical potential appears at the terminals of two electrodes involved in the process. The theoretical value of the fuel cell potential is 1.25 V, which matches that of NiCd and NiH_2 batteries. Multiple fuel cells are stacked in series–parallel combinations using heavy graphite pallets for the required voltage and current, just as the electrochemical cells are in a battery. However, as soon as the current is drawn, the voltage drops significantly due to various losses. Because the primary loss mechanism is ohmic loss in the electrodes, the voltage continues to drop with increasing current. The voltage drop is given by $V_{drop} = (\alpha + \beta \ln J)$, where J is current density at the

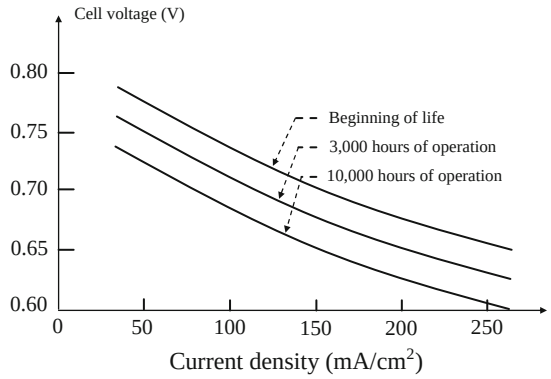

Fig. 10.27 Fuel cell output voltage versus current density and operating hours

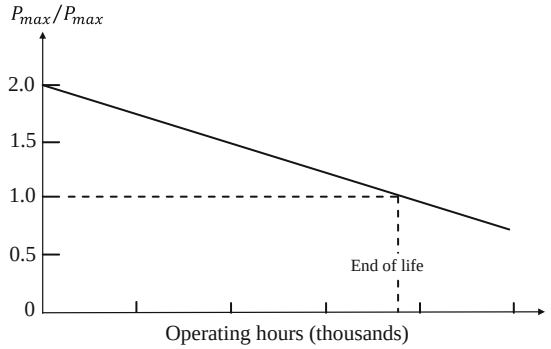

Fig. 10.28 P_{max}/P_{max} ratio versus time in operating hours determines fuel cell life

electrode surface, and α and β are constants which depend on temperature and the electrode surface.

The theoretical potential difference of 1.25 V between the anode and cathode in the hydrogen–oxygen fuel cell is determined by the difference of the free energy of the reaction product and the fuel and oxidant. This potential is different in different fuel cells depending on the reactions involved. The electrical performance of a fuel cell is represented by the electrode voltage versus surface current density, commonly known as the polarization curve or V–I curve. Ideally, a single H_2–O_2 fuel cell could produce 1.25 V DC at ambient conditions. Undesirable ions and products of the intermediate irreversible reactions decrease the cell potential, even at open circuit. Further voltage drop under load results from various irreversible polarizations in the cell. The net result of these polarizations is that the practical fuel cell produces between 0.5 and 1.0 V DC at currents of 100–400 mA/cm^2 of cell area. Fuel cell performance can be increased by increasing the cell temperature and reactant partial pressure. A trade-off exists between achieving higher performance by operating at higher temperature or pressure and confronting the materials and hardware problems imposed at more severe conditions.

The practical operating range of the fuel cell is controlled by ohmic loss. The V–I characteristic in this region is very similar to that of a battery, except that the average discharge voltage is lower. The voltage drops approximately linearly with increasing current and also with time, as shown in Fig. 10.27 [16]. At any given time, the terminal V–I relationship can be expressed as $V = V_0 - kI$, where V_0 is the open circuit voltage and k is a constant. The value of k increases and V_0 decreases with time. The power at any operating point is given by $P = VI = [(V_0 - kI)(V_0 - V)/k]$. The maximum power is when $dP/dt = 0$, which occurs at $V = 1/2V_0$, leading to

$$P_{max} = \frac{V_0^2}{4k}. \tag{10.11}$$

Table 10.8 Comparison of the performance of various fuel cell

Fuel cell technology	Specific power (W/kg)	Life in hours
Alkaline	100–150	~50,000
Solid polymer	100–150	~50,000
Alkaline (space shuttle)	300–400	3,000–5,000
Lightweight cell under development	600–700	TBD

Unlike the PV cell, the fuel cell does not work in *use the input energy or lose it* mode. It uses the on-board fuel to generate power. For this reason, the fuel cell is not operated at P_{max} until it approaches the end of life. It is rather operated at the maximum fuel efficiency until the EOL.

As V_0 degrades with time, so does P_{max}. The open circuit voltage can be expressed as a function of time as $V_0(t) = V_0(0) - K_0h$, where h is the hours since the fuel cell was placed in operation. With a voltage regulating converter between the fuel cell and the load, the life of the fuel cell can be defined as the time it takes for the voltage to decay below the required input voltage, for P_{max} to fall below the required output power. It can be predicted from the V_0 versus time relation. The expected life of the fuel cell is determined as shown in Fig. 10.28 [16].

The performance of various types of fuel cell for space applications is compared in Table 10.8. Compared to a PV array, the fuel cell gives much higher power per kilogram. Flexibility is another major advantage, as it does not need Sun pointing and provides the same power during both day and night. Its disadvantage is that it needs to carry fuel on-board.

10.4.7 Beam Power Satellite

The traditional power system in space uses a solar array and a battery for each satellite. The concept of using a centralized large power-satellite (powersat) has been receiving

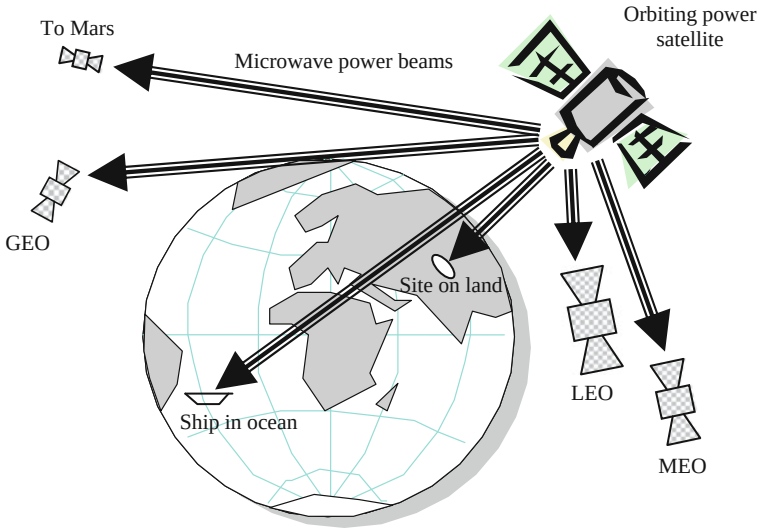

Fig. 10.29 Power transmission from central power satellite to multiple satellites

seed funding at NASA for some time. In this concept, depicted in Fig. 10.29, a high-power satellite generates bulk power, which is then transmitted to multiple satellites by laser or microwave beams. The electric propulsion of a spacecraft using beam power from a powersat is also possible. The beam power can also be used for rescue operation in remote regions of Earth, or anywhere in the ocean. The advantages of a central power satellite transmitting beam power to a number of user spacecraft are

- Large PV arrays are replaced by a much smaller power-receiving antenna in the user spacecraft.
- A significantly smaller battery can replace larger batteries as proper orientation with the power satellite(s) will avoid satellite-to-satellite eclipses.
- Longer mission life since the spacecraft life is not limited by its solar array or battery.
- Provides large peak power if and when needed, such as for electric propulsion, thus significantly decreasing the on-board fuel mass.
- Orienting the spacecraft to the powersat beam is much simpler than to orienting to the Sun.

10.4.7.1 Microwave Beam

The power transmission efficiency in space by a microwave beam is given by Lineberry and Chapman [17]

$$\eta = 1 - e^{-\frac{A_t A_r}{d^2 \lambda^2}} \tag{10.12}$$

where, η is the fraction of the transmitted power captured by the receiving antenna, A_t, A_r is the transmitter and receiver antenna area, respectively, d is the distance between the transmitter and receiver, and λ is the wavelength of the microwave power beam. The distance between the powersat and the user satellite may vary. The microwave transmission may be effectively used over short distances. The frequencies considered for such systems are from 3 to 300 GHz [18] with the corresponding wavelengths from 100 down to 1 mm.

In 2003, an experiment was planned using the Cosmos-1 solar sail, at 800 km altitude, to transmit power by a microwave beam from the Goldstone 100 m antenna. The Goldstone steerable dish radiates up to 1/2 MW power; it was estimated the sail would to receive only 1,700 W. The resulting microwave pressure was estimated to accelerate the sail by 10^{-7} g and demonstrate the principle of beaming power to a spacecraft. The acceleration of the sail would have depended only on power and not on the frequency of the beam, however the experiment was not conducted due a failure of the Cosmos-1 launch vehicle. In another experiment at JPL and the University of California at Irvine, a 10 kW, 7-GHz microwave beam in vacuum chamber produced a power density of 1 kW/cm^2 to heat a sail surface to 2,000 K.

Microwave transmitters have been under developments much longer than lasers. They are far more efficient and cost much less. They do not damage the receiving surface as lasers can, and do not refract while passing through air. However, microwaves require much larger antennas for the same focusing ability.

10.4.7.2 Laser Beam

Laser beams may be more efficient over long distances in the 10,000–50,000 km range [19]. The laser system consist of three parts

- First the solar energy collected on the powersat is converted into laser beam using a solid-state solar pumped laser. It consists of a crystal placed in the focus of a parabolic solar concentrator.
- The monochromatic laser radiation is then focused into a beam using an optical mirror of appropriate size. The wavelength of such a laser is equal to 1.06 μm, and the

conversion efficiency 20–25 %. A focused power laser beam then transmits the power to the user satellite or a rescue site on the Earth at 80–90 % efficiency.

- Finally, the received energy is converted into electrical power using the conventional PV cell. The conversion efficiency of a PV cell under laser illumination is around 50 %. The maximum electrical power output of the silicon PV cell using such a system can be 3,000 W/m^2 from laser radiation compared to 300 W/m^2 from natural solar radiation. The solar array requirement on the user satellite is thus greatly reduced, and the battery can be eliminated by avoiding powersat-to-user satellite eclipses.

A powersat, once developed and built, could make the user satellite much lighter and less expensive, so that many could be launched at lower cost per launch. This could open up entirely new kinds of missions in Earth orbit and in interplanetary space at much less incremental cost. The concept is like the 19th century railroad system. Once the tracks are laid, the train itself is a small added expense.

10.4.7.3 Space-to-Ground Power

Driven by the environmental and depletion concerns of the fossil energy sources, the U.S. Department of Energy, NASA and ESA have funded space-based generation of power for ground use. The equivalent mass density of air on Earth with typical moisture and pollution is 1.5 times that of pure air. The solar radiation on a normal Earth surface with air mass 1.5 (AM 1.5) is about 1 kW/m^2. With 12-hour nights on average, seasonal Sun variations, and overcasts, the annual average energy yield of a ground-based PV system may be around 6 kWh/m^2 per day. A 400 MW power station on the ground using 20 % efficient PV cells would need 40 million square meters of PV array. Storing sufficient energy to last 5 days without Sun would require 60,000 MWh of energy storage assuming 80 % round trip energy efficiency. A space-based system can reduce the collector area to 1/4th and eliminate the need of energy storage by making the beam power dispatchable on demand.

The performance of a solar array placed on the Earth's surface versus in LEO and GEO is summarized in Table 10.9. It shows that the energy collection per square meter in space is several times higher than that on Earth. Furthermore, it is 50 % higher in GEO than in LEO. One concept study has considered a medium Earth orbit at around 10,000 km altitude for such a powersat for ground use.

Ambitious proposals have been explored for harnessing solar energy for terrestrial use by deploying solar powersats in GEO that could generate power 24 h a day, 365 days a year. One concept study has shown that one satellite with a 146 km^2 solar array could deliver power equivalent to 10 nuclear power plants on Earth. The 1 km^2 antenna would transmit power in a sharp 2.4 GHz microwave beam to an Earth receiving station. Here, it would be converted into DC and inverted into 10,000 MW 60 Hz AC and delivered to the distribution system of the electrical power utility. The basic converter would use inductors (perhaps superconducting) to store the energy and boost the voltage.

Table 10.9 Performance of solar array placed on ground and in LEO and GEO

Solar array location	Earth	LEO	GEO
Air mass	1.5 with average moisture and pollution	0	0
Solar radiation (W/m^2)	1,000 in full Sun 500 in partial Sun	1,350	1,350
Incident energy (kWh/m^2 per year)	1,643	7,884	11,826
Useful sunlight (h/day)	6 on average	16	24
Launch and maintenance cost in orbit	0	Medium	High

In the proposed concept, the beamed power is converted to 60 or 50 Hz utility power using high voltage converters. Massive series–parallel connections of numerous converters would be needed to beam gigawatts of power to Earth from space [20]. The space-to-space power transmission would be at low level in W/m^2, while the space-to-ground power transmission would be in hundreds of W/m^2. However, a U.S. government regulation limits the microwave radiation to 110 W/m^2. Therefore, the hundreds of W/m^2 beam intensity would require a regulation change or special permission to beam to a remote location from where it would be transmitted to populated load centers. This high beam intensity is still a several times lower than the natural Sun intensity of 1,000 W/m^2 on the ground. Whether it would pose a cancer risk to humans has yet to be resolved.

Several innovative concepts are being studied for collecting solar energy in space and transmitting microwave beams to other spacecraft that may be orbiting the Earth, on an interplanetary mission, or on a planetary surface. NASA's Solar Space Power Exploratory Research and Technology program is investigating systems at power levels ranging from 100 kW to 1,200 MW. The building blocks of such a system are

- A large Sun-oriented solar array that tracks the Sun and generates power at high voltage in the 400–1,000 V range.
- A rotating microwave transmitter in space that tracks a receiving antenna (rectenna)/rectifier station on Earth.
- A microwave beam at several GHz frequency, using solid-state power converters, magnetrons, or klystrons.
- A rotary joint between the solar collector and the transmitter.

- High voltage cables.
- DC to microwave power converters in space and microwave to DC power converters and DC to 50 or 60 Hz AC inverters on the ground.

A concept study for delivering 1,200 MW from GEO to the ground grid has developed the following estimates [21]

- A solar array with 4–5 concentration ratio with futuristic conversion efficiency of 39 % generating at specific power of 1,000 W/kg and 550 W/m^2 at 1,000 V.
- A 5.8 GHz microwave beam of Gaussian power density distribution with 10 dB taper from the transmitter center to the edge.
- Solid-state transmitters operating at 80 V and the solar array at 1,000 V.
- Power distribution from solar array at 100 kV, so that converters are needed at both ends of the distribution lines. These converters substantially add into the system mass. Using 6,000 V magnetrons and reducing the distribution voltage to 6,000 V could eliminate the transmission voltage converters.
- A rectenna size on Earth about 7,450 m in diameter.
- Overall wireless power transmitting efficiency around 35 %.
- A system for 1,200 MW power to the grid requires a solar array of 7,300,000 m^2 area, equating to a 2,700 × 2,700 m^2 or 3 km diameter array in space. The rectenna on the ground is estimated to be 44,000,000 m^2 area or 7.5 km diameter. The ground receiver would be about six times the solar array area because of (a) power losses in various components, and (b) the beam power density being limited under the federal regulation on microwave power.
- The mass of the above concept satellite is estimated to be 22,500–30,000 metric tons at launch and 17,000–22,000 metric tons in orbit. A great many technology developments and demonstration are needed to make the cost per kWh delivered to the ground competitive with the conventional ground-based grid power [22–24].

Acknowledgments Several figures and tables in this chapter are reproduced with permission from Patel, M. R., "Spacecraft Power Systems", CRC Press, 2005. The author is also grateful to two industry experts for reviewing the manuscripts and providing valuable feedbacks. They are Mr. James E. Haines, retired head of power system group of European Space Agency, and Mr. Abbas Salim, retired senior staff engineer of Lockheed Martin Corporation.

References

1. Hyder, A. K. et al., *"Spacecraft Power Technologies,"* Imperial College Press/World Scientific Publishing, London, 2003.
2. Marshall, C. G. et al., "Example of a prototype lightweight solar array and the three promising technologies it incorporates," *Proceedings of the 35th Intersociety Energy Conversion Engineering Conference*, SAE, 1999, Paper No. 01-2550.
3. Frohlich, R. C., *"Contemporary measures of the solar constant: The solar output and its variations,"* Colorado Associated University Press, Boulder, CO, 1977, pp. 93-109.
4. Green, M.A., Emery, K., Hishikawa, Y., Warta, W., Dunlop, E.D. 2011. Solar cell efficiency tables (Version 38), Progress in Photovoltaics: Research and Applications 19, 565-572.
5. Parez, M. E. et al., "Energy storage for space applications," *Proceedings of the 36th Intersociety Energy Conversion Engineering Conference*, ASME, 2001, pp. 85-89.
6. Hojnicki, J. S. et al., "Space Station Freedom Electrical Performance Model," NASA Glenn Research Center, Report No. TM-106395, 1993.
7. Haines, J. E., "Inner Planets sample return missions, the challenge for power systems," *Proceedings of the 34th Intersociety Energy Conversion Engineering Conference,* SAE, 1999, Paper No. 2483.
8. Brandhorst, Jr, H. W. and Chen, Z., "PV approaches for near-Sun missions," *Proceedings of the 34th Intersociety Energy Conversion Engineering Conference,* SAE, 1999, Paper No. 2631.
9. Choi, M. K., "Power and thermal systems with thermoelectric generators at 930°C for solar probe inside 0.1 au," *Proceedings of the 36th Intersociety Energy Conversion Engineering Conference*, ASME, 2001, Vol. II, pp. 1161-63.
10. Elbuluk, M. E. et al., "Low temperature performance evaluation of battery management technologies," *Proceedings of the 34th Intersociety Energy Conversion Engineering Conference*, SAE, 1999, Paper No.01-2543.
11. Nagasubramanian, G, "Low temperature electrical performance characteristic of Li-Ion cells," *Proceedings of the 34th Intersociety Energy Conversion Engineering Conference*, SAE, 1999, Paper No. 01-2462.
12. Croft, H., Staniewicz, R., Smart, M. C., and Ratnakumar, B. V., "Cycling and low temperature performance operation of Li-ion cells," *Proceedings of the 35th Intersociety Energy Conversion Engineering Conference,* AIAA, 2000, Paper No. 27-AP-B1.
13. Smart, M. C, Huang, C. K., Ratnakumar, B. V., Surampudi, S., and Sakamoto, J. S., "Factors affecting Li-Ion cell performance," Proceedings of the 37th Power Sources Conference, Paper No. 239, 1996.
14. Mason, L. S., "A solar dynamic power option for space solar power," *Proceedings of the 34th Intersociety Energy Conversion Engineering Conference,* SAE, 1999, Paper No. 01-2601.
15. Oman, H., "Fuel cells power for aerospace vehicles," *IEEE Aerospace and Electronics System Magazine,* Vol. 17, No. 2, February 2002, pp. 35-41.
16. Babasaki, T., Take, T., and Yamashita, T., "Diagnosis of fuel cell deterioration using fuel cell current-voltage characteristics," Proceedings *of the 34th Intersociety Energy Conversion Engineering Conference,* SAE, 1999, Paper No. 01-2575.
17. Lineberry, J. T. and Chapman, J. N., "MHD Augmentation of rocket engine for space propulsion," *Proceedings of the 35th Intersociety Energy Conversion Engineering Conference,* AIAA, 2000, Paper No. 3056.
18. Koert, P. and Cha, J. T., "Millimeter Wave Technology for Spec Power Beaming," *IEEE Transactions on Microwave Theory and Technology*, Vol. 40, No. 6, June 1992, pp. 1251-58.
19. Grechnev, A. B. et al., "Centralized power as basis of new philosophy of space power engineering," *Proceedings of the 34th Intersociety Energy Conversion Engineering Conference,* SAE, 1999, Paper No. 2436.
20. Kusic, G., "Conversion of beamed microwave power," *Proceedings of the 35th Intersociety Energy Conversion Engineering Conference,* AIAA, 2000, Paper No. 3071.
21. SAIC and Futron Corporation, "Space Solar Power Concept Definition Study," NASA Report No. SAIC-99/1016, February 1999.

22. Mankins, J. C. and Howell, J., "Overview of the space solar power exploratory research and technology program," *Proceedings of the 35th Intersociety Energy Conversion Engineering Conference, AIAA, 2000,* Paper No. 3060.
23. Carrington, C. et al., "The abacus/reflector and integrated symmetrical concentrator concept for space power collection and transmission," *Proceedings of the 35th Intersociety Energy Conversion Engineering Conference, AIAA, 2000,* Paper No. 3067.
24. Lynch, T. H., "Sun tower PMAD architecture," Proceedings of the 34th Intersociety Energy Conversion Engineering Conference, SAE, 1999, Paper No. 2441.

Further Reading

25. Patel, M.R., "Spacecraft Power Systems", CRC Press, Boca Raton, 2005.
26. Hyder, A. K. et al., *"Spacecraft Power Technologies,"* Imperial College Press/World Scientific Publishing, London, 2003.